Multistable mode of second harmonic generation in photonic crystal with combined nonlinear response

Vyacheslav A. Trofimov
Tatiana M. Lysak
Lomonosov Moscow State University
Moscow 119992
Russian Federation
E-mail: vatro@cs.msu.su

Sheng Lan
South China Normal University
Laboratory of Photonic Information Technology
Guangzhou 510006, China

Abstract. Second harmonic generation (SHG) of femtosecond pulses in layered photonic crystal with combined nonlinearity is analyzed. Within the approximation of plane wave, the problem under consideration is solved analytically. One shows the possibility of a multistable mode of frequency conversion that occurs due to self-action of laser pulses because of cubic susceptibility. Dependence of the number of solutions on parameters of the problem is discussed and demonstrated. On the basis of the obtained analytical solution, the possible modes of frequency conversion are found out. To verify and prove the realization of obtained analytical results, a computer simulation on the basis of Schrödinger equations is made. This comparison demonstrates good agreement between the analytical solution and computer simulation during a definite time interval, depending on thickness of layers of the photonic crystal and wavelength of laser radiation.
[DOI: 10.1117/1.3609798]

Subject terms: photonic crystals; quadratic and cubic nonlinear responses; second harmonic generation; bistability; femtosecond pulse.

Paper 10117R received Jan. 10, 2011; revised manuscript received Jun. 15, 2011; accepted for publication Jun. 20, 2011; published online Aug. 16, 2011.

1 Introduction

At present, photonic crystals are being widely investigated in the world in various aspects of their interaction with laser radiation. In particular, great attention is attracted to second harmonic generation (SHG) in photonic crystals. With this aim, one considers crystals with defects[1–3] and one-,[1–17] and two-dimensional[18–26] periodic structures with nonlinear response. Basically, modern investigations have revealed the various mechanisms for the possibility of SHG efficiency enhancement: in the vicinity of the defect,[1–3] near the edge of photonic bandgap,[6,7] and due to the special choice of propagation parameters.[8–10,13–15,24,25] Solitons and solitary waves in photonic crystals are also of great interest.[11,12,21–23] Further research in this direction require investigation of the influence of nonlinearities and dielectric permittivities and sizes of photonic crystal elements on considering process and require construction of photonic crystals with required properties. For example, in Refs. 18–20 the radial structures to support second harmonic (SH) Bessel beams and other multiple processes for the purpose of cascading, nonlinear beam shaping, and nonlinear polarization switching are designed.

It is obvious that qualitative analysis of the system of nonlinear equations, which describe the interaction of a femtosecond pulse with nonlinear photonic crystal, can clarify an opportunity of achievement for requiring characteristics of process under analysis. Thus, in previous papers,[28,29] we have solved the SHG problem in homogeneous media with cubic and quadratic nonlinear response in the framework of long pulse duration and plane-wave approximation. It should be stressed that such a combined response of the medium appears for nonsymmetric crystal [for example, potassium dideuterium phosphate (DKDP crystal) or lithium triborate (LBO crystal)] with quadratic susceptibility at SHG of high-intensity femtosecond laser pulse and they are well known in the literature.[30–33] In dependence of the crystal, the power density of laser pulse, at which the combined response takes place, occurs from 80 GW/sm^2. However, in Ref. 2 it was shown that the quadratic response in photonic crystal appears also in the centrosymmetric medium. We analyze the SHG in a layered structure, which consists of layers with different dielectric permittivities and quadratic susceptibilities.

The main feature of our approach is the use of invariants (conservation laws) of the problem to build the solution. As a result, several regimes of frequency conversion were found due to the parametrical analysis of the solution. Essentially, that computer simulation, made on the base of conservative finite difference schemes, gives the same results as the analytical ones under certain conditions. It is very important that a comparison of computer simulation results to the physical experiment showed a good agreement[33] between them. Note, as well, that without using the invariants it is impossible to write an analytical solution of considered equations.

In this paper, the same approach is used for the analysis of SHG in photonic crystals with combined nonlinearity. We obtain the analytical solution of this problem and investigate possible regimes of frequency conversion as well as conditions for their realization. Among them we stress the bistability regime, the regime of unchanging initial intensities of waves, and the regime of full conversion of the energy for fundamental wave. It is essential that without cubic susceptibility the appearance of bistable regime of SHG is impossible.

At the bistability regime, the generation of doubled-frequency waves with either low or high efficiency is possible. It takes place, for example, when both waves at basic and double frequency fall on the crystal. In this case, the realization of low- or high-efficiency conversion of energy of the basic wave depends on initial amplitudes of interacting waves

0091-3286/2011/$25.00 © 2011 SPIE

and on the difference of their phases. Nevertheless, there is an opportunity to achieve a highly efficient regime of frequency conversion for the practically important case of the absence of an input wave at double frequency. It should be mentioned that the investigation of dependence of the regimes on the phase difference is very important for practical purposes. For the example, it is necessary for the visualization of the terahertz laser radiation.[34–36] There are also another two parameters that determine a realization of mentioned regimes of frequency conversion. The first one is the ratio of dimensionless parameters, which is defined by quadratic and cubic nonlinearities that characterize conversion of the energy of the waves and their self-action. The second is the ratio of dielectric permittivities, which determine wave-vector mismatch of interacting waves.

All analytical expressions derived in the paper are confirmed by computer simulation on the basis of nonlinear Schrödinger equations for interaction of laser radiation with 1-D photonic crystal. We show how to obtain the required regime of generation using the results of our analytical research.

2 Basic Equations

The case of laser pulse interaction with photonic-crystals that we consider here is shown in Fig. 1. To write equations that describe a femtosecond pulse propagation in layered photonic crystal, we used the approach proposed in Ref. 27. The main feature of this approach is the refusal from preferential direction of laser pulse propagation. Here, we apply this approach to describe the interaction of two laser pulses in 2-D (layered) photonic crystal, taking into account the wave-vector mismatch between propagating waves.

As is well known, the propagation of laser pulse is described by the wave equation

$$\frac{\partial^2 E}{\partial z^2}+\frac{\partial^2 E}{\partial x^2}-\frac{1}{c^2}\frac{\partial^2 E}{\partial t^2}=\frac{4\pi}{c^2}\frac{\partial^2 P}{\partial t^2}, \quad 0<z<L_z,$$
$$0<x<L_x,\ 0<t<L_t. \tag{1}$$

Here, $E(x,z,t)$ is the strength of the electrical field; $P(x,z,t)$ is the polarization of the medium; x and z are the space coordinates along the layers of photonic crystal and perpendicular to them, correspondingly; t is the time coordinate; L_z and L_x are the lengths of the domain, which contain, in particular,

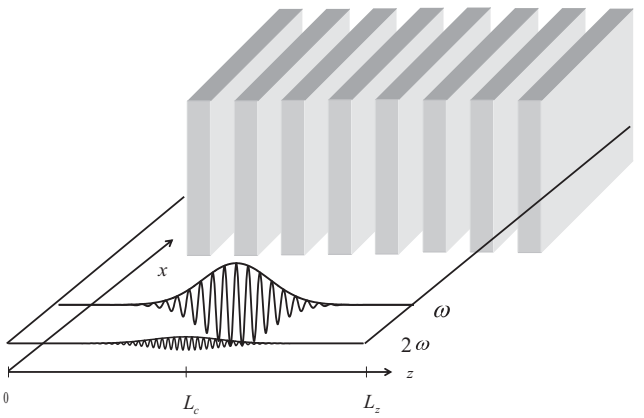

Fig. 1 Scheme of the laser pulse interaction with layered photonic crystal.

the photonic crystal (Fig. 1); L_t is the time interval under consideration; and c is the light velocity in vacuum. It is well known that a response of the medium on the frequency ω at propagation of the high-intensity femtosecond laser pulse is written as follows:

$$P=\chi^{(1)}(x,z)E+\chi^{(2)}(x,z)E^2+\chi^{(3)}(x,z)E^3, \tag{2}$$

$\chi^{(1)}$, $\chi^{(2)}$, $\chi^{(3)}$ are the linear, quadratic, and cubic susceptibilities of the medium, correspondingly.

To describe SHG, one introduces slow varying complex amplitudes in time on the fundamental frequency $\omega_1=\omega$ and on the double frequency $\omega_2=2\omega$ as

$$E_j(z,t)=0.5\{\tilde{\tilde{A}}_j(z,t)\exp[i(\omega_j t-k_j z)]+c.c.\},\quad j=1,2, \tag{3}$$

where c.c. denotes a conjugation of complex functions and k_j is a wavenumber of corresponding wave. The expressions for k_j are the following:

$$k_j=\frac{\sqrt{\varepsilon(\omega_j,x,z)}\omega_j}{c},\quad j=1,2.$$

Thus, we take into account the dispersion of substance at a propagation of the laser pulse in a layered structure. It is necessary to emphasize that the dependence of group velocity from dielectric permittivity of layers and light frequency is considered by us at computer simulation. Influence of the periodic structure on the laser radiation propagation arises from a presence in equations written below the parameter describing the frequency of the structure. The second-order dispersion is not ingenuously included in equations. Nevertheless, we take into account the diffraction of light in the propagation direction. In linear case of light propagation, this is the equivalent of consideration of second-order dispersion of a laser pulse.

Substituting Eq. (3) into Eq. (1) and neglecting the second derivatives on time $\partial^2\tilde{\tilde{A}}_j/\partial t^2$ within the chosen approximation on the first step of writing the mathematical model, one obtains the following set of equations for complex amplitudes of waves on fundamental and double frequencies:

$$\frac{\partial^2\tilde{\tilde{A}}_1}{\partial x^2}+\frac{\partial^2\tilde{\tilde{A}}_1}{\partial z^2}-2ik_1\frac{\partial\tilde{\tilde{A}}_1}{\partial x}-i\varepsilon(\omega_1,x,z)\frac{2\omega_1}{c^2}\frac{\partial\tilde{\tilde{A}}_1}{\partial t}$$
$$+\left[\frac{\varepsilon(\omega_1,x,z)\omega_1^2}{c^2}-k_1^2\right]\tilde{\tilde{A}}_1+\frac{4\pi\chi^{(2)}(x,z)}{c^2}\omega_1^2\tilde{\tilde{A}}_1^{\,*}\tilde{\tilde{A}}_2e^{-i\Delta kx}$$
$$+\frac{3\pi\chi^{(3)}(x,z)}{c^2}\omega_1^2\tilde{\tilde{A}}_1(|\tilde{\tilde{A}}_1|^2+2|\tilde{\tilde{A}}_2|^2)=0,$$
$$\frac{\partial^2\tilde{\tilde{A}}_2}{\partial x^2}+\frac{\partial^2\tilde{\tilde{A}}_2}{\partial z^2}-2ik_2\frac{\partial\tilde{\tilde{A}}_2}{\partial x}-i\varepsilon(\omega_2,x,z)\frac{2\omega_2}{c^2}\frac{\partial\tilde{\tilde{A}}_2}{\partial t}$$
$$+\left[\frac{\varepsilon(\omega_2,x,z)\omega_2^2}{c^2}-k_2^2\right]\tilde{\tilde{A}}_2+\frac{2\pi\chi^{(2)}(x,z)}{c^2}\omega_2^2\tilde{\tilde{A}}_1^{\,2}e^{i\Delta kx}$$
$$+\frac{3\pi\chi^{(3)}(x,z)}{c^2}\omega_2^2\tilde{\tilde{A}}_2(|\tilde{\tilde{A}}_2|^2+2|\tilde{\tilde{A}}_1|^2)=0,$$
$$0<t\le L_t,\quad 0<x<L_x,\quad 0<z<L_z, \tag{4}$$

with the initial distribution of the amplitudes

$$\tilde{\tilde{A}}_j(x,z,t=0)=\tilde{A}_{j0}A_{0j}(x,z),\quad j=1,2,$$

$$0 \le x \le L_x, \quad 0 \le z \le L_z,$$

and zero-value boundary conditions

$$\tilde{\tilde{A}}_j(x, z=0, t) = \tilde{\tilde{A}}_j(x, z=L_z, t) = \tilde{\tilde{A}}_j(x=0, z, t) = \tilde{\tilde{A}}_j(x=L_x, z, t) = 0.$$

where $\tilde{A}_{j0}$ is the square root of maximal intensity of the corresponding wave, $\varepsilon(\omega_j,x,z) = 1 + 4\pi\chi^{(1)}\varepsilon(\omega_j,x,z)$, $\Delta k = k_2 - 2k_1$ is the mismatch of wave-vectors. At writing of Eqs. (4), as usual, we neglected the dependence of $\chi^{(2)}$ and $\chi^{(3)}$ on the frequency. Also as usual, the mismatching of wave-vectors appears in Eq. (4) as the exponential factor.

The next step is made with the aim of simplification of Eqs. (4) for computer simulation. Using some algebra, we remove the first derivative on x coordinate in Schrödinger equations. In this case, one of the invariants (conservation laws) of Eqs. (4) will be self-valid for any finite difference schemes. With this aim, multiplying the first of Eqs. (4) by $\exp(-k_1x)$ and the second one by $\exp(-k_2x)$ and then introducing the new variables

$$\tilde{A}_1(x,z,t) = \tilde{\tilde{A}}_1(x,z,t)\exp(-ik_1x) \text{ and } \tilde{A}_2(x,z,t) = \tilde{\tilde{A}}_2(x,z,t)\exp(-ik_2x),$$

we get the following equations:

$$i\varepsilon(\omega_1,x,z)\frac{2\omega_1}{c^2}\frac{\partial\tilde{A}_1}{\partial t} + \frac{\partial^2\tilde{A}_1}{\partial x^2} + \frac{\partial^2\tilde{A}_1}{\partial z^2} - \frac{\varepsilon(\omega_1,x,z)\omega_1^2}{c^2}\tilde{A}_1 + \frac{4\pi\chi^{(2)}(x,z)}{c^2}\omega_1^2\tilde{A}_1^*\tilde{A}_2 + \frac{3\pi\chi^{(3)}(x,z)}{c^2} \times \omega_1^2\tilde{A}_1(|\tilde{A}_1|^2 + 2|\tilde{A}_2|^2) = 0,$$

$$i\varepsilon(\omega_2,x,z)\frac{2\omega_2}{c^2}\frac{\partial\tilde{A}_2}{\partial t} + \frac{\partial^2\tilde{A}_2}{\partial x^2} + \frac{\partial^2\tilde{A}_2}{\partial z^2} - \frac{\varepsilon(\omega_2,x,z)\omega_2^2}{c^2}\tilde{A}_2 + \frac{2\pi\chi^{(2)}(x,z)}{c^2}\omega_2^2\tilde{A}_1^2 + \frac{3\pi\chi^{(3)}(x,z)}{c^2}\omega_2^2\tilde{A}_2(|\tilde{A}_2|^2 + 2|\tilde{A}_1|^2) = 0, \quad 0 < x < L_x, \quad 0 < z < L_z, \tag{5}$$

with the initial distribution of amplitudes

$$\tilde{A}_j(x,z,t=0) = \tilde{A}_{j0}A_{0j}(x,z)e^{-ik_jx}, \quad j = 1,2, \quad 0 \le x \le L_x, \quad 0 \le z \le L_z.$$

For application of Eqs. (5), it is necessary to answer the main question, which is, what terms in new equations describe the wave-vector mismatching? We discuss this question next.

Because we consider a layered structure on the z coordinate and homogeneous structure on the x coordinate (1-D photonic crystal) with two different layers, which lengths are denoted as d_1' and d_2' and dielectric permittivities equal to ε_{11}, ε_{12} and ε_{21}, ε_{22} on frequencies ω_1 and ω_2 correspondingly for each layer, let us define, for convenience, the parameter $d = (d_1' + d_2')/4$, which characterizes the periodic structure of photonic crystal. It is necessary to stress that, in this case, the optical properties of medium are the same in any section of x coordinate. Hence, the following relations are valid:

$$\varepsilon(\omega_j,x',z') = \varepsilon(\omega_j,z'), \quad \chi^{(s)}(x',z') = \chi^{(s)}(z'), \quad j = 1,2, \quad s = 1,2,3.$$

Introducing the dimensionless variables

$$z' = \frac{z}{d}, \quad x' = \frac{x}{d}, \quad t' = t\frac{c}{d}, \quad \bar{k}_j = k_jd, \quad j = 1,2, \quad \bar{L}_x = \frac{L_x}{d}, \quad \bar{L}_z = \frac{L_z}{d}, \quad \bar{L}_t = \frac{cL_t}{d}, \quad \bar{A}_j(x',z',t') = \frac{\tilde{A}_j(x',z',t')}{A_{\text{nor}}}, \quad A_{j0} = \frac{\tilde{A}_{j0}}{A_{\text{nor}}}, \quad j = 1,2,$$

where $A_{\text{nor}} = \sqrt{I_{\text{nor}}}$ and I_{nor} is an intensity of normalization, we get from Eq. (5) the following set of equations:

$$\varepsilon(\omega_1,z')\frac{\partial\bar{A}_1}{\partial t'} + iD\left(\frac{\partial^2\bar{A}_1}{\partial x'^2} + \frac{\partial^2\bar{A}_1}{\partial z'^2}\right) + i\beta\gamma(z')\bar{A}_1^*\bar{A}_2 + i\beta[\varepsilon(\omega_1,z') + \alpha(z')(|\bar{A}_1|^2 + 2|\bar{A}_2|^2)]\bar{A}_1 = 0,$$

$$\varepsilon(\omega_2,z')\frac{\partial\bar{A}_2}{\partial t'} + i\frac{D}{2}\left(\frac{\partial^2\bar{A}_2}{\partial x'^2} + \frac{\partial^2\bar{A}_2}{\partial z'^2}\right) + i\beta\gamma(z')\bar{A}_1^2 + i2\beta[\varepsilon(\omega_2,z') + \alpha(z')(|\bar{A}_2|^2 + 2|\bar{A}_1|^2)]\bar{A}_2 = 0, \quad 0 < x' < L_x, \quad 0 < z' < \bar{L}_z, \quad 0 < t \le \bar{L}_t,$$

with the initial distribution of complex amplitudes

$$\bar{A}_j(x',z',t'=0) = A_{j0}A_0(x',z')e^{-i\bar{k}_jx'}, \quad j = 1,2, \quad 0 \le x' \le \bar{L}_x, \quad 0 \le z' \le \bar{L}_z.$$

In the above set of equations, other notations are defined as

$$D = \frac{1}{4\pi\Omega}, \quad \beta = \pi\Omega, \quad \Omega = \frac{d\omega_1}{2\pi c} = \frac{d}{\lambda_1}, \quad \gamma(z') = 4\pi\chi^{(2)}(z')A_{\text{nor}}, \quad \alpha(z') = 3\pi\chi^{(3)}(z')A_{\text{nor}}^2,$$

where $\lambda_1 = 2\pi c/\omega_1$ is a wavelength of the fundamental wave, and we have taken into account the relationship between frequencies of interacting waves $\omega_2 = 2\omega_1$.

As we consider a two-layer structure, let us introduce parameters α_1, γ_1 and α_2, γ_2 as values of $\alpha(z)$ and $\gamma(z)$ in two different layers.

The last step is an introduction of the following functions:

$$A_1(x',z',t') = \bar{A}_1(x',z',t')\exp(i\beta t'), \quad A_2(x',z',t') = \bar{A}_2(x',z',t')\exp(i2\beta t'),$$

and omitting the accents at z' and t' and line at another variable as well. Thus, one obtains the following equations, which are written in a final form, for describing the femtosecond laser pulse propagation in photonic crystal with quadratic and cubic nonlinear response:

$$\varepsilon(\omega_1,z)\frac{\partial A_1}{\partial t} + iD\left(\frac{\partial^2A_1}{\partial x^2} + \frac{\partial^2A_1}{\partial z^2}\right) + i\beta\gamma(z)A_1^*A_2 + i\beta\alpha(z)A_1(|A_1|^2 + 2|A_2|^2) = 0$$

$$\varepsilon(\omega_2,z)\frac{\partial A_2}{\partial t} + i\frac{D}{2}\left(\frac{\partial^2A_2}{\partial x^2} + \frac{\partial^2A_2}{\partial z^2}\right) + i\beta\gamma(z)A_1^2 + i2\beta\alpha(z)A_2(|A_2|^2 + 2|A_1|^2) = 0, \quad 0 < t \le L_t, \quad 0 < x < L_x, \quad 0 < z < L_z, \tag{6}$$

with the initial distributions of complex amplitudes:

$$A_1(x,z,t=0) = A_{10}A_{01}(x,z)e^{-i\sqrt{\varepsilon(\omega_1,z)}2\pi\Omega[x-(L_x/2)]},$$
$$A_2(x,z,t=0) = A_{20}A_{02}(x,z)e^{-i\sqrt{\varepsilon(\omega_2,z)}4\pi\Omega[x-(L_x/2)]},$$
$$0 \le x \le L_x, \quad 0 \le z \le L_z. \tag{7}$$

These initial conditions correspond to a propagation of laser pulses along the x coordinate.

Note that Eq. (6) with initial conditions [Eq. (7)] describes the interaction with mismatch of wave-vectors also if $\varepsilon(\omega_1,z)$ is not equal to $\varepsilon(\omega_2,z)$. Indeed, taking into account the expressions for k_1, k_2 the mismatching of wave-vectors of interacting waves can be written as follows:

$$\Delta k = (k_2 - 2k_1)d = \frac{2\omega_1 d}{c}\left[\sqrt{\varepsilon(\omega_2,z)} - \sqrt{\varepsilon(\omega_1,z)}\right]$$
$$= 4\pi\Omega\left[\sqrt{\varepsilon(\omega_2,z)} - \sqrt{\varepsilon(\omega_1,z)}\right]. \tag{8}$$

Let us stress that the set of Eqs. (6) have not been met in the previous papers.

If $A_{20} = 0$ (this case is very important for practice), then only a laser pulse on the fundamental frequency falls on the photonic crystal and SHG takes place in the photonic crystal. In the case of nonzero A_{20}, a wave propagation on the doubling frequency first occurs in a homogeneous medium before the photonic crystal, for example, and then both waves interact in photonic crystal.

Thus, this written set of equations contains all the features of well-known equations describing the SHG. Thus, equations that are used by us are more convenient for computer simulations because the first derivative on x coordinate is absent in our equations, and one of the invariants of the equations are self-valid.

3 Plane-Wave Approximation

Many features of the SHG process by femtosecond pulses in photonic crystal can be analyzed in the framework of plane waves approximation, suggesting $D \to 0$, which is valid for large-enough values of Ω and/or for small intervals of time for observation. In this case, the second terms in Eqs. (6) can be neglected and laser pulses interaction in each point of photonic crystal can be described by the first-order differential equations,

$$\varepsilon(\omega_1)\frac{dA_1}{dt} + i\beta\gamma A_1^* A_2 + i\beta\alpha A_1(|A_1|^2 + 2|A_2|^2) = 0,$$
$$0 < t \le L_t,$$
$$\varepsilon(\omega_2)\frac{dA_2}{dt} + i\beta\gamma A_1^2 + i2\beta\alpha A_2(|A_2|^2 + 2|A_1|^2) = 0. \tag{9}$$

Note that in Eq. (9), the values of $\varepsilon(\omega_1) = \varepsilon_1 = \{\varepsilon_{11},\varepsilon_{12}\}$, $\varepsilon(\omega_2) = \varepsilon_2 = \{\varepsilon_{21},\varepsilon_{22}\}$, $\alpha = \{\alpha_1, \alpha_2\}$, $\gamma = \{\gamma_1,\gamma_2\}$ and the evolution of complex amplitudes as a consequence, depends on the z coordinate, parametrically. For brevity, we do not write this dependence in the functions, keeping it in mind.

Let us introduce real functions: amplitudes a_j and phases φ_j of the fundamental and SH waves as

$$A_j = a_j e^{i\varphi_j}, \quad j = 1, 2.$$

In this case the Eq. (9) can be rewritten as follows:

$$\varepsilon_1\frac{da_1}{dt} = \beta\gamma a_1 a_2 \sin\varphi, \quad \varepsilon_2\frac{da_2}{dt} = -\beta\gamma a_1^2 \sin\varphi,$$
$$\frac{d\varphi}{dt} = -2\frac{\beta\alpha}{\varepsilon_1\varepsilon_2}\left[(\varepsilon_1 - 2\varepsilon_2)a_2^2 - (\varepsilon_2 - 2\varepsilon_1)a_1^2\right]$$
$$-\frac{\beta\gamma}{\varepsilon_1\varepsilon_2}\cos\varphi\left(\varepsilon_1\frac{a_1^2}{a_2} - 2\varepsilon_2 a_2\right), \quad \varphi = \varphi_2 - 2\varphi_1, \tag{10}$$

with initial conditions

$$a_2|_{t=0} = a_{20}, \quad a_1|_{t=0} = a_{10}, \quad \varphi|_{t=0} = \varphi_0.$$

For Eqs. (10), the following invariants are valid

$$I_1 = a_1^2 + a_2^2\frac{\varepsilon_2}{\varepsilon_1} = a_1^2 + a_2^2 s,$$
$$I_3 = 2\gamma\beta a_2 a_1^2\cos\varphi + \alpha\beta(|a_1|^4 + |a_2|^4 + 4|a_1|^2|a_2|^2), \tag{11}$$

or in other notations (introducing the modified third invariant $\bar{\bar{I}}_3$),

$$\bar{\bar{I}}_3 = I_3 - \alpha\beta I_1^2$$
$$= a_2\left[2\beta\gamma a_1^2\cos\varphi + 2\beta\alpha a_1^2 a_2(2-s) + \beta\alpha a_2^3(1-s^2)\right], \tag{12}$$

where $s = \varepsilon_2/\varepsilon_1$ is a function of the z coordinate. Comparing the parameter s and Eq. (8), it becomes clear the parameter s characterizes mismatching of wave-vectors.

For the further analysis, it is convenient to introduce the new parameter $q = \gamma/\alpha$ and to rewrite the invariant

$$\tilde{I}_3 = \bar{\bar{I}}_3/(\beta\alpha) = a_2\left[2qa_1^2\cos\varphi + 2a_1^2 a_2(2-s) + a_2^3(1-s^2)\right]. \tag{13}$$

Combining the invariants I_1, $\tilde{I}_3$, and the first Eq. (10), we obtain an equation for the normalized intensity $P_1 = a_1^2/I_1$ at the fundamental wave. Obviously, from the first invariant in Eq. (11) one gets the normalized intensity $P_2 = a_2^2/I_1 = (1 - P_1)/s$ for the double-frequency wave. Thus, we multiply the first equation from the system in Eq. (10) by a_1 and derive the expression

$$\cos\varphi = \frac{\tilde{I}_3 - a_2^2\left[2a_1^2(2-s) + a_2^2(1-s^2)\right]}{2a_1^2 a_2 q} \tag{14}$$

from the invariant in Eq. (13). Then we divide the numerator and denominator in Eq. (14) by I_1^2 and, employing the trigonometric formulas and expression for the first invariant in Eq. (11), we get the following dependence:

$$\sin\varphi = \frac{\sqrt{\varepsilon_1\varepsilon_2}\dfrac{dP_1}{dt}}{2\gamma\beta\sqrt{I_1}P_1\sqrt{1-P_1}}$$
$$= \pm\sqrt{1 - \left\{\frac{\frac{\tilde{I}_3}{I_1^2} - (1-P_1)\frac{1}{s}\left[2P_1(2-s) + (1-P_1)\frac{1}{s}(1-s^2)\right]}{2P_1\sqrt{1-P_1}\sqrt{\frac{1}{s}}\frac{q}{\sqrt{I_1}}}\right\}^2} \tag{15}$$

from the first equation of Eq. (10).

Integrate two last parts of Eq. (15) by t, and write the equation with respect to intensity of the fundamental wave as:

$$\int_{(P_1)_0}^{P_1} \frac{dx}{\sqrt{4x^2(1-x)\left(\frac{q}{\sqrt{I_1}}\right)^2 s^3 - \left\{\frac{\tilde{I}_3}{I_1^2}s^2 - (1-x)[1-s^2-x(s^2-4s+1)]\right\}^2}} = \int_{(P_1)_0}^{P_1} \frac{dx}{\sqrt{f(x)}} = \pm\frac{\alpha\beta I_1}{s\varepsilon_2}t + C. \quad (16)$$

The plus or minus sign in Eq. (16) is chosen in accordance of initial values of $(P_1)_0$ and φ_0: "+" should be chosen for $0 < \varphi_0 < \pi$ and "−" for $\pi < \varphi_0 < 2\pi$. For $\varphi_0 = 0$ and $\varphi_0 = 2\pi$, an additional analysis should be made (we present it in Sec. 4). Note that the integral in Eq. (16) is an elliptical one. Its form (and, consequently, the frequency conversion regime) is governed by the relationship between the constants s, $q/\sqrt{I_1}$ and $\tilde{I}_3/I_1^2$. Mention, that initial values $(P_1)_0$ and $(P_2)_0$ of fundamental and double-frequency waves meet the equality

$$(P_1)_0 + (P_2)_0\, s = 1,$$

which follows from the first invariant (11).

4 Analysis of Elliptical Integral

Obviously, solution of the problem depends on properties of polynomial $f(x)$, which are specified by parameters s, q, initial amplitudes of waves a_{10}, a_{20} and phase difference φ_0. There are two main differences between the considered case and the case investigated in Ref. 29. First, the coefficient ($r = (s^2 - 4s + 1)^2$ at the high power in the polynomial $f(x)$ depends on the parameter s and may be equal to zero. Thus, it is necessary to consider two different cases: (i) $r = 0$ and (i) $r \neq 0$. Thus, polynomial $f(x)$ may have two, three, or four real roots.

Second, in contrast to the previously considered case, the value of the first invariant I_1 depends on parameter s, if a_{20} is not equal to zero. Because of this dependence on parameter s, we have chosen a normalization of waves amplitudes that is different from amplitudes values. In the opposite case under the investigation of frequency conversion regimes on the plane (q,s), we deal with the situation when parameter q should also depend on s through dependence of I_1 from the input intensities of double-frequency wave. Obviously, it is not convenient for analysis.

4.1 *Regions of Various Regimes of Frequency Conversion on the Plane of Parameters (q,s)*

First of all, note that our analysis can be confined to the case $a_{10}^2 + a_{20}^2 = 1$. Indeed, it is easy to see that the regions on the plane (q,s) for the arbitrary initial amplitudes a'_{10}, a'_{20} are similar ones for $a_{10} = a'_{10}/\sqrt{A}$, $a_{20} = a'_{20}/\sqrt{A}$, where $a'_{10} + a'_{20} = A$. They are only stretched or compressed along the q-axis by $a_{10}/a'_{10} = \sqrt{A}$ times. However, at constant value of the parameter q, the regions of various solutions depend on initial amplitudes (a_{01}, a_{02}) of the waves.

The dependence of the parameter q on the laser light intensity gives us the opportunity to take into account waveguide loss. In this case, the corresponding point on the plane (q,s) continuosly moves along horizontal line toward bigger values of parameter q as time grows. Thus, if the point at the initial time moment is in the bistability region, then it moves into region 1 and 2, correspondingly, or straight into region 2 in the dependence of absorption coefficient of medium.

Sub-regions on the plane (q,s), corresponding to various numbers and properties of the roots (positive, negative, complex, etc.) of the polynomial $f(x)$, are shown in Figs. 2 and 3. Note, that all real roots of polynomial $f(x)$ are ≤ 1. Indeed, from Eq. (16) one follows that $f(x)$ is <0 for $x > 1$ and hence cannot be equal to zero.

Our analysis shows, that despite the values of a_{10}, a_{20}, and φ_0, three regions are distinguished in the plane (q,s). For parameters in region 3 there are four real positive roots of the polynomial $f(x)$. Hence, the bistability regime takes place and each pair of roots defines the possible intensity range for frequency conversion. These regimes differ in efficiency and will refer to them as high- and low-efficiency ones. It is very important that, for these regimes, the difference of phases and invariants of interacting waves are the same. It gives one the opportunity to switch from one regime to another. Thus, region 3 can be divided into two subregions, which are denoted as 3.1 and 3.2. Note that bistability regime cannot be realized if the ratio of dielectric permittivities on the fundamental and double frequencies does not belong to the interval $2 - \sqrt{3} < s < 2 + \sqrt{3}$.

For parameters in region 2, there are two positive and two negative roots. In this case, the two positive roots define maximal and minimal intensities in the limits of which the solution is changing in time. While for parameters in region 1, only two real roots take place, both of them being positive. In contrast to Ref. 29, in region 1 there are two subregions that do not intersect. One of these subregions lies in the band $2 - \sqrt{3} < s < 2 + \sqrt{3}$, and the other satisfies $s < 2 - \sqrt{3}$. If the difference of phase for interacting waves is equals to $\varphi_0 = 0,\pi$ the curve, named curve 3, appears in the plane (q,s). For parameters in this curve, the initial wave amplitudes do not change in time. Essentially, for $\varphi_0 \neq 0,\pi$ such curve is absent.

Figure 2 shows the typical configuration of the regions for $\varphi_0 = 0,\pi$ and for values of φ_0 from the interval $(0,\pi)$, as well as for the practically important case of the absence of the SH wave $a_{20} = 0$ at the initial moment. Evolution of the regions with φ_0, varying from 0 to π, for small ($a_{20} = 0.2$; Fig. 2, left half) and big ($a_{20} = 0.8$; Fig. 2, right half) initial amplitudes of the second harmonic wave is shown in Fig. 3. (Note that we consider the case $a_{10}^2 + a_{20}^2 = 1$.) Note also that, for considered parameters a_{20}, φ_0, all the previously described

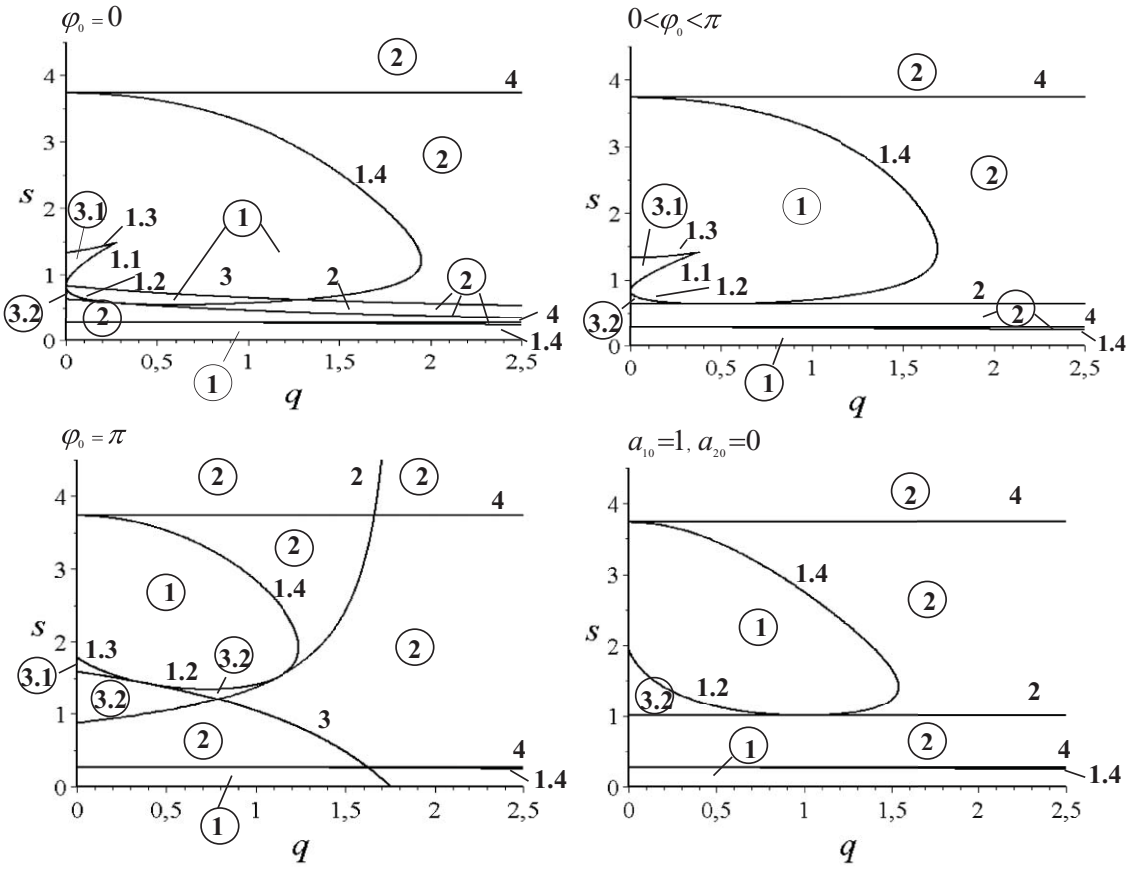

Fig. 2 Regions (denoted as numbers in circles), corresponding to different modes of SHG and their boundaries (denoted as numbers without circles) on the plane of parameters (q,s) for the following values of difference of phases of interacting waves and amplitude of second harmonics (φ_0, a_{20}) = (π/2;0.8), (0;0.8), (π,0.4). Region 3 corresponds to the bistability mode and is divided into two subregions: the high-efficient regime of SHG is realized in subregion 3.1 and the low-efficient regime of SHG is realized in subregion 3.2. For parameters from regions 1 and 2, the unique mode of SHG takes place, while analytical solutions in these areas are different.

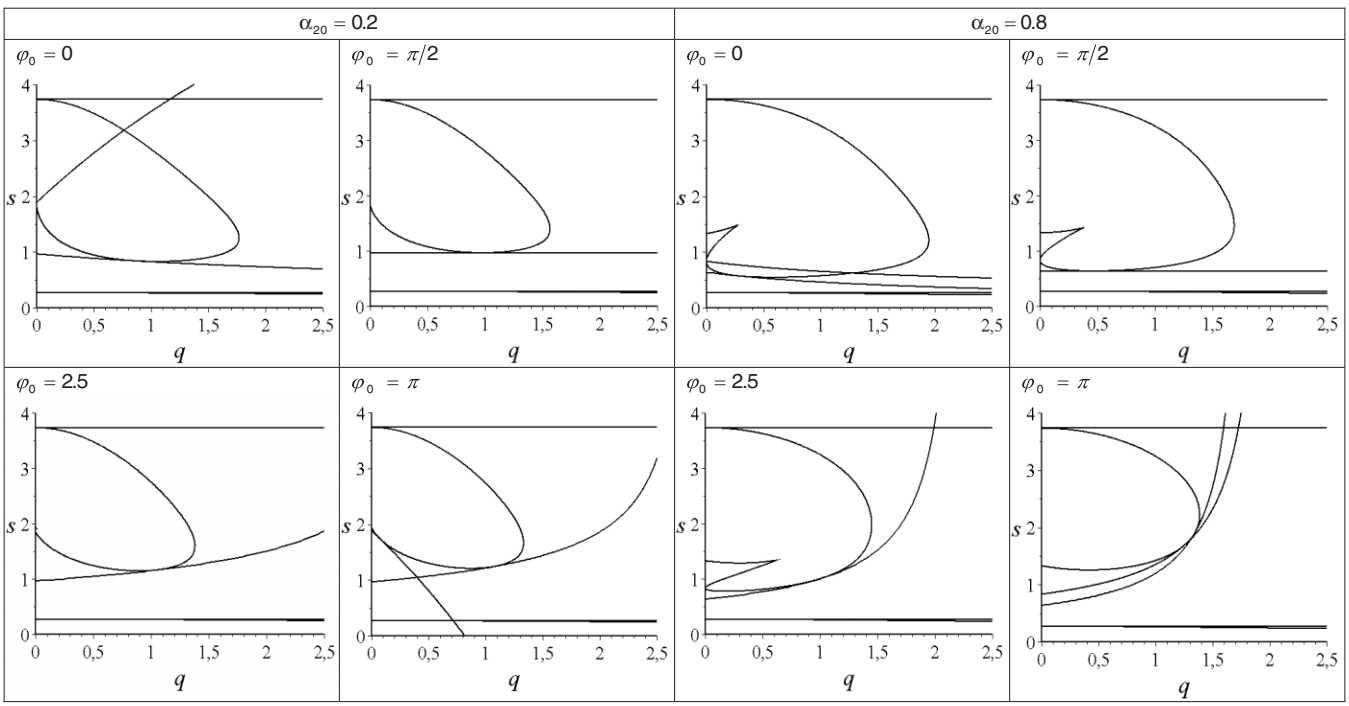

Fig. 3 Transformation of regions of different modes of SHG (Fig. 2) on the plane (q,s) in dependence on initial phase difference for $a_{20} = 0.2$ and $a_{20} = 0.8$.

regions exist in the plane (q,s). Although the configuration of their boundaries depends on the initial amplitudes and phase difference of waves. Evolution of P_1 for parameters from different regions and boundaries of these regions is depicted in Fig. 4. Let us discuss the main features of the regions.

Thus, as was already mentioned, if the values of parameter s do not meet the inequalities $2-\sqrt{3} < s < 2+\sqrt{3}$, then the bistable regime of the frequency conversion (region 3) cannot be realized. The range of the values q,s for realization of the bistable regime becomes narrower as parameter $q = \gamma/\alpha$ grows, and it vanishes for the respectively small self-action. On the contrary, 100% energy conversion takes place only for the relatively small values of self-action (curve 2). The regime of unchanging initial intensities (curve 3) becomes possible only for the initial phase difference φ_0 equal to 0 or π. While for zero values of φ_0 this regime is stable for all possible parameters of its realization, at $\varphi_0 = \pi$ the stability of this regime takes place only for the self-action, which is small enough when compared to the coefficient of coupling of interacting waves. As the initial intensity of the fundamental wave grows, the critical value of self-action for the stability of the regime of unchanging initial intensities decreases (compare Fig. 3 for $a_{20} = 0.2$ and $a_{20} = 0.8$).

Essentially, for the initial intensity of the fundamental wave many times greater than the intensity of SH ($a_{10} \gg a_{20}$), the subregion of the high-efficiency generation (subregion 3.1) is practically absent (Fig. 3). The growth of initial phase difference φ_0 results in the increase of region 3. This is most pronounced for the small initial values of the fundamental wave intensity a_{10}^2. On the contrary, the part of region 1 that lies in the band $2-\sqrt{3} < s < 2+\sqrt{3}$ is shrinking significantly along the axis of parameter q, as the initial phase difference φ_0 grows.

Let us also stress the difference of the region configuration for the case of zero and nonzero initial amplitude of the SH wave (Fig. 2). Thus, regime of unchanging initial amplitudes is unavailable for zero initial SH wave [curve 3 is absent in the plane (q,s)]. Subregion 3.1 of region 3 (the subregion of high-effective generation) is also absent, similar to the case of small SH initial amplitude (Fig. 3, left half), which means impossibility for realization of high-efficiency generation. Curve 2 turns into a line, and full energy conversion is possible only for parameters that meet the equality $s = 1$ and inequality $q > 1$, simultaneously. Bistability regime cannot take place, if parameter s does not satisfy inequalities $1 < s < 2+\sqrt{3}$.

4.2 *Analytical Solution for Pure Cubic and Quadratic Nonlinearities*

Before we consider the general case, let us focus on some important particular cases.

4.2.1 *Analytical solution for pure quadratic nonlinearity: Case $a_{20} \neq 0$*

The case of pure quadratic nonlinearity ($\alpha = 0$, $\gamma \neq 0$) has already been investigated.[37] In this case, the second invariant in Eqs. (11), (14), and (16) can be rewritten as follows:

$$I_3 = 2\gamma\beta a_2 a_1^2 \cos\varphi, \qquad \cos\varphi = \frac{I_3}{2a_1^2 a_2 \gamma\beta},$$

$$\int_{(P_1)_0}^{P_1} \frac{dx}{\sqrt{4x^2(1-x)(\gamma/\sqrt{I_1})^2 s^3 - \left[\left(I_3/\beta I_1^2\right)s^2\right]^2}} = \int_{(P_1)_0}^{P_1} \frac{dx}{\sqrt{f(x)}} = \pm\frac{\beta I_1}{s\varepsilon_2}t + C,$$

consequently. The last equations can take the form

$$\int_{(P_1)_0}^{P_1} \frac{dx}{\sqrt{x^2(1-x)-\tilde{\kappa}}} = \pm\frac{2\beta\gamma\sqrt{I_1}}{\sqrt{\varepsilon_1\varepsilon_2}}t + C,$$

$$\tilde{\kappa} = \cos^2\varphi_0 \frac{(a_{20}/a_{10})^2 s}{[1+(a_{20}/a_{10})^2 s]^3}.$$

It is well seen from the last expression that the inequality $\tilde{\kappa} \le (4/27)$ is valid for all possible a_{10}, a_{20} and φ_0. Hence, the polynomial $f(x)$ has three real roots $(P_1)_1$, $(P_1)_2$, $(P_1)_3$: two of them are positive and one is negative. From the analyses of the polynomial $f(x)$, it follows that $P_1(t)$ belongs to the interval between the positive roots: $(P_1)_3 < 0 < (P_1)_2 \le P_1(t) \le (P_1)_1 < 1$.

In this case, the evolution $P_1(t)$ oscillates [Fig. 4(a)] and is described by an elliptical sine,

$$P_1(t) = (P_1)_1 - h^2[(P_1)_1 - (P_1)_2],$$

$$h = sn\left[\frac{\beta\gamma\sqrt{I_1}}{\sqrt{\varepsilon_1\varepsilon_2}}\sqrt{(P_1)_1-(P_1)_3}\,t - t'\middle| m\right],$$

$$t' = F(\theta_0|m)\begin{cases} 1, & 0 \le \varphi_0 < \pi \\ -1, & \pi \le \varphi_0 < 2\pi \end{cases},$$

$$\theta_0 = \arcsin\sqrt{\frac{(P_1)_1-(P_1)_0}{(P_1)_1-(P_1)_2}}, \quad m = \frac{(P_1)_1-(P_1)_2}{\left[(P_1)_1-(P_1)_3\right]},$$

with the half-period of oscillation as follows:

$$\bar{t} = \frac{\sqrt{\varepsilon_1\varepsilon_2}}{\beta\gamma\sqrt{I_1}}\frac{K(m)}{\sqrt{(P_1)_1-(P_1)_3}}.$$

In the degenerate case, when the initial intensities a_{10}, a_{20} and phase difference of waves φ_0 is governed by the equalities

$$\varphi_0 = 0 \quad \text{or} \quad \varphi_0 = \pi \quad \text{and} \quad \left(\frac{a_{20}}{a_{10}}\right)^2 s = \frac{1}{2},$$

equality $\tilde{\kappa} = 4/27$ takes place and two positive roots coincide: $(P_1)_3 < 0 < (P_1)_2 = P_1(t) = (P_1)_1 < 1$. In this case, initial intensities preserve their values.

4.2.2 *Analytical solution for pure quadratic nonlinearity: Case $a_{20} = 0$*

The other degenerate case corresponds to the zero initial amplitude of the second harmonic wave: $a_{20} = 0$. In this case, an equation for the normalized intensity P_1 can be obtained from the following consideration. We divide the third equation [Eq. (10)] by the first one,

$$\frac{d\varphi}{da_1} = -ctg\varphi\frac{a_1^2 - 2sa_2^2}{sa_1a_2^2}$$

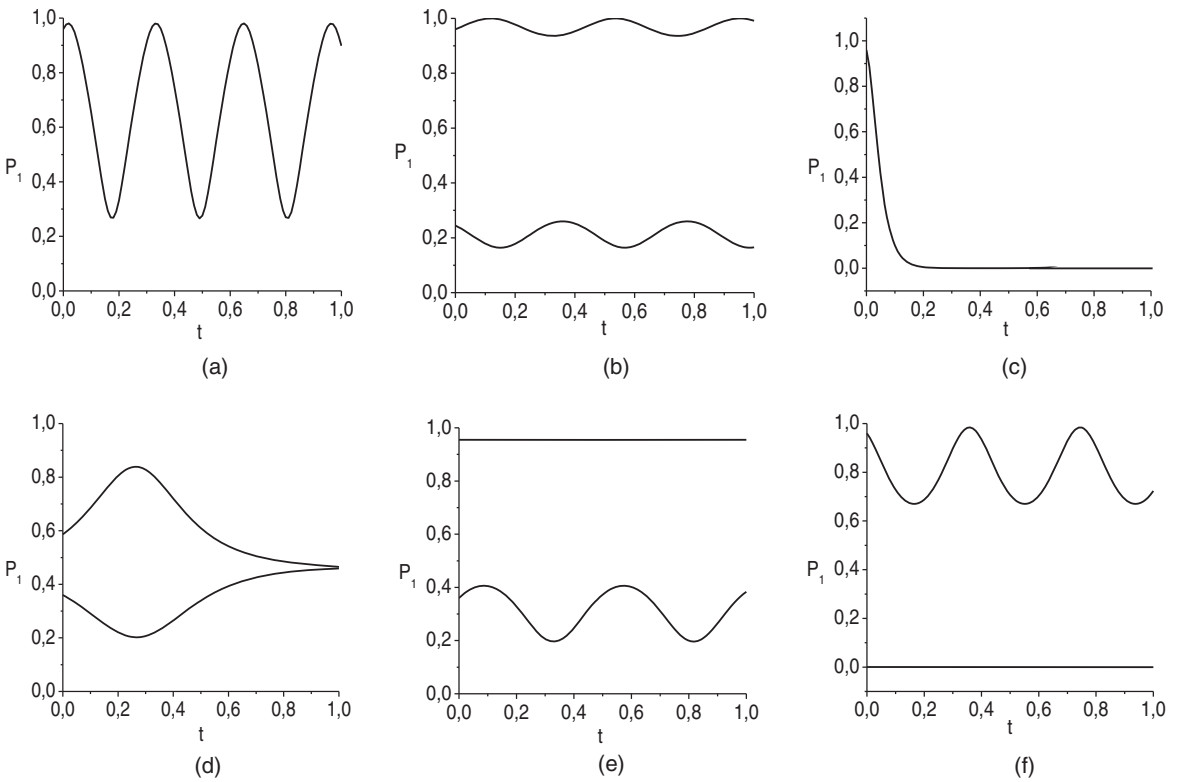

Fig. 4 Evolution of normalized intensity of the fundamental wave in time for the parameters from the following regions shown in Fig. 2: (a) regions 1, 2, and the boundary 1.4 between these regions; (b) region 3 of bistability regime; (c) curve 2 of the full energy conversion, belonging to the region 2; (d) boundaries 1.1, 1.2; (e) boundary 1.3 between the regions 3 and 1; (f) boundary between regions 3 and 2 and curve 3 in region 3.2.

and derive the following invariant:

$$\cos\varphi\sqrt{s}a_2a_1^2 = \cos\varphi_0\sqrt{s}a_{20}a_{10}^2$$

from this equation. Taking into account $a_{20} = 0$, we conclude $\cos\varphi = 0$ and $\sin\varphi = -1$ {case $\sin\varphi = 1$ results in negative values of a_2 from the second Eq. (10), which contradicts determination of a_2 as nonnegative quantity}. Thus, from the first Eq. (10), we obtain the following equation for P_1:

$$\int_{(P_1)_0}^{P_1} \frac{dx}{\sqrt{x^2(1-x)}} = \int_{(P_1)_0}^{P_1} \frac{dx}{\sqrt{f(x)}} = -\frac{2\beta\gamma\sqrt{I_1}}{\sqrt{\varepsilon_1\varepsilon_2}}t + C$$

The polynomial $f(x)$ has thus two zero and one positive roots $(P_1)_3 = 0 = (P_1)_2 \le P_1(t) \le (P_1)_1 = 1$ and the evolution $P_1(t)$ can be described by hyperbolic tangent

$$P_1(t) = 1 - h^2, \quad h = th\left(\frac{\beta\gamma\sqrt{I_1}}{\sqrt{\varepsilon_1\varepsilon_2}}t\right).$$

4.2.3 *Analytical solution for pure cubic nonlinearity*

As is well seen from Eqs. (10), in the case of pure cubic nonlinearity ($\alpha \neq 0$, $\gamma = 0$), amplitudes of both waves preserve their initial values. It should be mentioned that for parameters from the region of bistability 3, two possible modes of wave propagation occurs. The realization of these modes depends on subregion to which the parameters of laser pulse interaction belong: their initial intensities. Thus, in subregion 3.1 the intensity of the second wave is greater than the intensity of first wave. For subregion 3.2, the opposite relation of intensities takes place.

4.3 *Analytical Solution for Various Regions*

In this section, we give the analytical expressions for $P_1(t)$ from Eq. (16). Essentially, this expressions depend on the number and arrangement of the roots of polynomial, which are determined by parameters q,s, initial amplitudes a_{10}, a_{20} (if $a_{20} \neq 0$) and difference of phases φ_0. It should be emphasized once more that $P_1(t) + P_2(t) \cdot s = 1$.

Thus, for the region 1 (Figs. 2 and 3) the polynomial $f(x)$ has two real roots $(P_1)_1$ and $(P_1)_2$, which satisfy the inequality $0 < (P_1)_2 < (P_1)_1 < 1$. The normalized intensity $P_1(t)$ of the fundamental wave is located between the roots $(P_1)_2 \le P_1(t) \le (P_1)_1$ and oscillates periodically in time [Fig. 4] in accordance with the following expressions:

$$P_1(t) = \frac{(P_1)_2\, c\,(h-1) - (P_1)_1\, d(h+1)}{c\,(h-1) - d(h+1)},$$

$$h = cn\left(\frac{\alpha\beta I_1\,|r_0|}{\varepsilon_2}\sqrt{cd}\,t - t'\middle|m\right) \quad r_0 = \frac{s^2 - 4s + 1}{s},$$

$$t' = F(\theta_0\,|m)\begin{cases} 1, & 0 \le \varphi_0 < \pi \\ -1, & \pi \le \varphi_0 < 2\pi \end{cases},$$

$$\theta_0 = \arccos\frac{[(P_1)_0 - (P_1)_2]c - [(P_1)_1 - (P_1)_0]d}{[(P_1)_0 - (P_1)_2]c + [(P_1)_1 - (P_1)_0]d},$$

$$F(\psi\,|m) = \int_0^{\psi} \frac{d\theta}{\sqrt{1 - m\sin^2\theta}}, \tag{17}$$

where $F(\psi|m)$ is an incomplete elliptic integral of the first kind and $cn(t|m)$ is the elliptic cosine. Parameters m, c, and d in Eq. (17) are related with the roots of the polynomial $f(x)$ in Eq. (16) as follows:

$$m = \frac{cd + [(P_1)_3 - (P_1)_2][(P_1)_1 - (P_1)_3] - (P_1)_4^2}{2cd}$$
$$c = \sqrt{[(P_1)_1 - (P_1)_3]^2 + (P_1)_4^2}, \quad d = \sqrt{[(P_1)_2 - (P_1)_3]^2 + (P_1)_4^2}. \tag{18}$$

Note that $(P_1)_3 \pm i(P_1)_4$ are the complex roots.

The moments of the reaching of extreme values (maximums and minimums) of P_1 are spaced by multiples of

$$\bar{t} = \frac{K(m)}{(\alpha\beta I_1 |r_0| / \varepsilon_2)\sqrt{cd}},$$

where $K(m) = F[(\pi/2)|m]$ is a complete elliptical integral of the first kind. Therefore, $\bar{t}$ is the half-period of the intensity oscillations.

In regions 2 and 3, the polynomial $f(x)$ has four real roots $(P_1)_1$, $(P_1)_2$, $(P_1)_3$, and $(P_1)_4$. Note that in region 2, only two of these roots have physical meaning because the other two are negative $(P_1)_4 < (P_1)_3 < 0 < (P_1)_2 < (P_1)_1 < 1$. However, in region 3, each of the roots has physical meaning and intensity of a fundamental wave can vary between the roots in the first or second pair, with the roots being renumbered in growing order. In both regions, the intensity $P_1(t)$ also oscillates in time [Figs. 4(a) and 4(b)]. Nevertheless, the expressions, which describe the evolution of intensity, are different in regions 2 and 3 and are different from corresponding expressions in region 1. Thus, the dependence $P_1(t)$ for the parameters from region 2 is described by an elliptical sine [Fig. 4(a)]

$$P_1(t) = \frac{(P_1)_1 [(P_1)_2 - (P_1)_4] + h^2 (P_1)_4 [(P_1)_1 - (P_1)_2]}{(P_1)_2 - (P_1)_4 + h^2 \left[(P_1)_1 - (P_1)_2\right]},$$
$$h = sn \left\{ \frac{\alpha\beta I_1 |r_0|}{2\varepsilon_2} \sqrt{[(P_1)_1 - (P_1)_3][(P_1)_2 - (P_1)_4]}\, t - t' \middle| m \right\}$$
$$t' = F(\theta_0 | m) \begin{cases} 1, & 0 \le \varphi_0 < \pi \\ -1, & \pi \le \varphi_0 < 2\pi \end{cases}, \tag{19}$$

$$\theta_0 = \arcsin \sqrt{\frac{[(P_1)_2 - (P_1)_4]\,[(P_1)_1 - (P_1)_0]}{[(P_1)_1 - (P_1)_2]\,[(P_1)_0 - (P_1)_4]}},$$
$$m = \frac{[(P_1)_1 - (P_1)_2][(P_1)_3 - (P_1)_4]}{[(P_1)_1 - (P_1)_3]\left[(P_1)_2 - (P_1)_4\right]}. \tag{20}$$

In this case, the half-period for changing of intensity is equal to

$$\bar{t} = \frac{2\varepsilon_2}{\alpha\beta I_1 |r_0|} \frac{K(m)}{\sqrt{[(P_1)_1 - (P_1)_3][(P_1)_2 - (P_1)_4]}}. \tag{21}$$

As was mentioned, in region 3 all the roots of the polynomial $f(x)$ are positive $0 < (P_1)_4 < (P_1)_3 < (P_1)_2 < (P_1)_1 < 1$. Hence, the two stable regimes of SHG take place [Fig. 4(b)]. Depending on the choice of initial intensities of interacting waves, one can realize for chosen q and s the high- or low-efficiency regime of frequency conversion. In subregion 3.1, inequalities $(P_1)_4 \le P_1(t) \le (P_1)_3$ take place and they correspond to SHG with high efficiency. The evolution of $P_1(t)$ in time is described by

$$P_1(t) = \frac{(P_1)_4[(P_1)_1 - (P_1)_3] + h^2 (P_1)_1[(P_1)_3 - (P_1)_4]}{(P_1)_1 - (P_1)_3 + h^2[(P_1)_3 - (P_1)_4]},$$
$$h = sn \left\{ \frac{\alpha\beta I_1 |r_0|}{2\varepsilon_2} \sqrt{[(P_1)_1 - (P_1)_3][(P_1)_2 - (P_1)_4]}\, t - t_2' | m \right\},$$
$$t_2' = F(\theta_0 | m) \begin{cases} -1, & 0 \le \varphi_0 < \pi \\ 1, & \pi \le \varphi_0 < 2\pi \end{cases},$$
$$\theta_0 = \arcsin \sqrt{\frac{[(P_1)_1 - (P_1)_3]}{[(P_1)_3 - (P_1)_4]} \frac{[(P_1)_0 - (P_1)_4]}{[(P_1)_1 - (P_1)_0]}}.$$

Half-period $\bar{t}$ of intensity oscillations and parameter m are determined by Eqs. (20) and (21).

For the other choice of a_{10}, corresponding to subregion 3.2, the intensity of the fundamental wave satisfies inequalities $(P_1)_2 \le P_1(t) \le (P_1)_1$ and the low-efficiency regime of SHG takes place. In this case, the evolution of the $P_1(t)$ case is determined by Eqs. (19)–(21) for region 2.

With respect to these regimes, two circumstances should be emphasized. The first is that the low-efficiency regime of frequency conversion is also possible for parameters q and s from the subregion 3.1 for the other initial conditions. Similarly, for the parameters from subregion 3.2, it is possible to achieve a high-efficiency regime. The second is a consequence of realization of the extreme intensities P_1 for the both regimes at the same time moments. As parameters s and q reach the values at the boundary with region 2, the ultimate intensities corresponding to the high- and low-efficiency regimes tend to be equal to the same value. However, the time moment $\bar{t}$ of its realization tends to infinity.

Other important results conclude in the impossibility of realizing the full energy conversion from the fundamental wave to the double-frequency wave for the parameters from regions 1 and 3. Next, we will show that, in contrast, this can take place for the parameters from region 2.

4.4 *Analytical Solution for Parameters from the Boundaries of the Regions*

For parameters from the boundaries of considered regions, the elliptical integral [Eq. (16)] can be reduced to the simple

tabular integrals. In this case, the intensity of the waves is described by elementary functions. Thus, for parameters from the boundary between regions 1 and 3 (curves 1.1, 1.2, and 1.3 in Figs. 2 and 3) four positive roots exist, similar to region 3. Nevertheless, unlike region 3, at least one pair of coinciding roots take place. In particular, for parameters q and s, which lie on curves 1.1 and 1.2, the inequalities $0 < (P_1)_4 < (P_1)_3 = (P_1)_2 < (P_1)_1 < 1$ are valid. That is why, similar to the case of region 3, two different (low- and high-efficiency) regimes of SHG take place. The evolution of intensity $P_1(t)$ in these regimes is described by the expressions

$$P_1^{(k)}(t) = \frac{(P_1)_2[(P_1)_1 - (P_1)_4]^2 - (-1)^k 2h\{(P_1)_4[(P_1)_1 - (P_1)_2] - (P_1)_1[(P_1)_2 - (P_1)_4]\} + (P_1)_2 h^2}{[(P_1)_1 - (P_1)_4]^2 - (-1)^k 2h\{[(P_1)_1 - (P_1)_2] - [(P_1)_2 - (P_1)_4]\} + h^2},$$

$$h = \exp\left\{\pm(-1)^k \frac{\alpha\beta I_1 |r_0|}{\varepsilon_2}\sqrt{[(P_1)_1 - (P_1)_2][(P_1)_2 - (P_1)_4]}\,t + t'\right\}, \quad \begin{cases} "+", & 0 \le \varphi_0 < \pi \\ "-", & \pi \le \varphi_0 < 2\pi \end{cases},$$

$$t' = \ln \frac{[\sqrt{[(P_1)_1 - (P_1)_2][(P_1)_0 - (P_1)_4]} - \sqrt{[(P_1)_2 - (P_1)_4][(P_1)_1 - (P_1)_0]}]^2}{|(P_1)_2 - (P_1)_0|} \quad k = 1, 2. \tag{22}$$

The first set of formulas ($k = 1$) describes the high-efficiency SHG, for which the choice of a_{10} results in validity of inequalities: $(P_1)_4 \le P_1(t) \le (P_1)_3$. This regime is realized for parameters at boundary 1.1. The other set ($k = 2$) corresponds to the low-efficiency SHG, so that the inequalities $(P_1)_3 \le P_1(t) \le (P_1)_1$ take place for corresponding choice of a_{10}. This regime is realized at curve 1.2. It should be stressed that the intensities in high- and low-efficiency regimes tend to each other exponentially with time growth [Fig. 4(d)]. As parameters cross boundaries 1.1 and 1.2, the regime of frequency conversion changes dramatically, being the result of merging (splitting) of high- and low-efficiency regimes. For example, Figs. 5(b) and 5(c) illustrate this situation. Abrupt growth/decrease of intensities is well seen at the small changes in dielectric permittivity ε_2 (parameter s) for both boundaries.

For parameters in the curve 1.3, due to the choice of a_{10}, the real roots of polynomial $f(x)$ and intensity of fundamental wave $P_1(t)$ are related as $0 < (P_1)_4 \le P_1(t) \le (P_1)_3 < (P_1)_2 = (P_1)_1 < 1$. Therefore, the high-efficiency regime of SHG takes place and is described by the following periodical function [Fig. 4(e)]:

$$P_1(t) = \frac{(P_1)_3[(P_1)_1 - (P_1)_4] + (P_1)_4[(P_1)_1 - (P_1)_3] - h(P_1)_1[(P_1)_3 - (P_1)_4]}{[(P_1)_1 - (P_1)_4] + [(P_1)_1 - (P_1)_3] - h[(P_1)_3 - (P_1)_4]},$$

$$h = \sin\left\{\pm\frac{\alpha\beta I_1 |r_0|}{\varepsilon_2}\sqrt{[(P_1)_1 - (P_1)_3][(P_1)_1 - (P_1)_4]}\,t + t'\right\}, \quad \begin{cases} "-", & 0 \le \varphi_0 < \pi \\ "+", & \pi \le \varphi_0 < 2\pi \end{cases},$$

$$t' = \arcsin \frac{[(P_1)_1 - (P_1)_4][(P_1)_3 - (P_1)_0] + [(P_1)_3 - (P_1)_1][(P_1)_0 - (P_1)_4]}{[(P_1)_1 - (P_1)_0][(P_1)_3 - (P_1)_4]}. \tag{23}$$

Then, the half-period of changing the intensity is expressed as

$$\bar{t} = \frac{\varepsilon_2}{\alpha\beta I_1 |r_0|} \frac{\pi}{\sqrt{[(P_1)_1 - (P_1)_3][(P_1)_1 - (P_1)_4]}}. \tag{24}$$

As can be well seen in Fig. 5(d), extreme intensities of the fundamental wave are changing smoothly at parameter values crossing boundary 1.3.

It is possible to choose other initial conditions a_{10}, a_{20}, and φ_0, so that for parameters from curve 1.3 takes place unchanging of initial amplitudes. These initial conditions correspond to the following arrangement of the roots and intensity: $0 < (P_1)_4 \le (P_1)_3 < (P_1)_2 = P_1(t) = (P_1)_1 < 1$. For example, this regime is shown in Fig. 5(e).

At the boundary between regions 1 and 2 (curve 1.4), as well as in region 2, only two positive roots of the polynomial $f(x)$ exist and the fundamental wave intensity is between them: $(P_1)_4 = (P_1)_3 < 0 < (P_1)_2 \le P_1(t) \le (P_1)_1 < 1$. That is why the full conversion of the energy of the fundamental wave into the energy of the double-frequency wave is

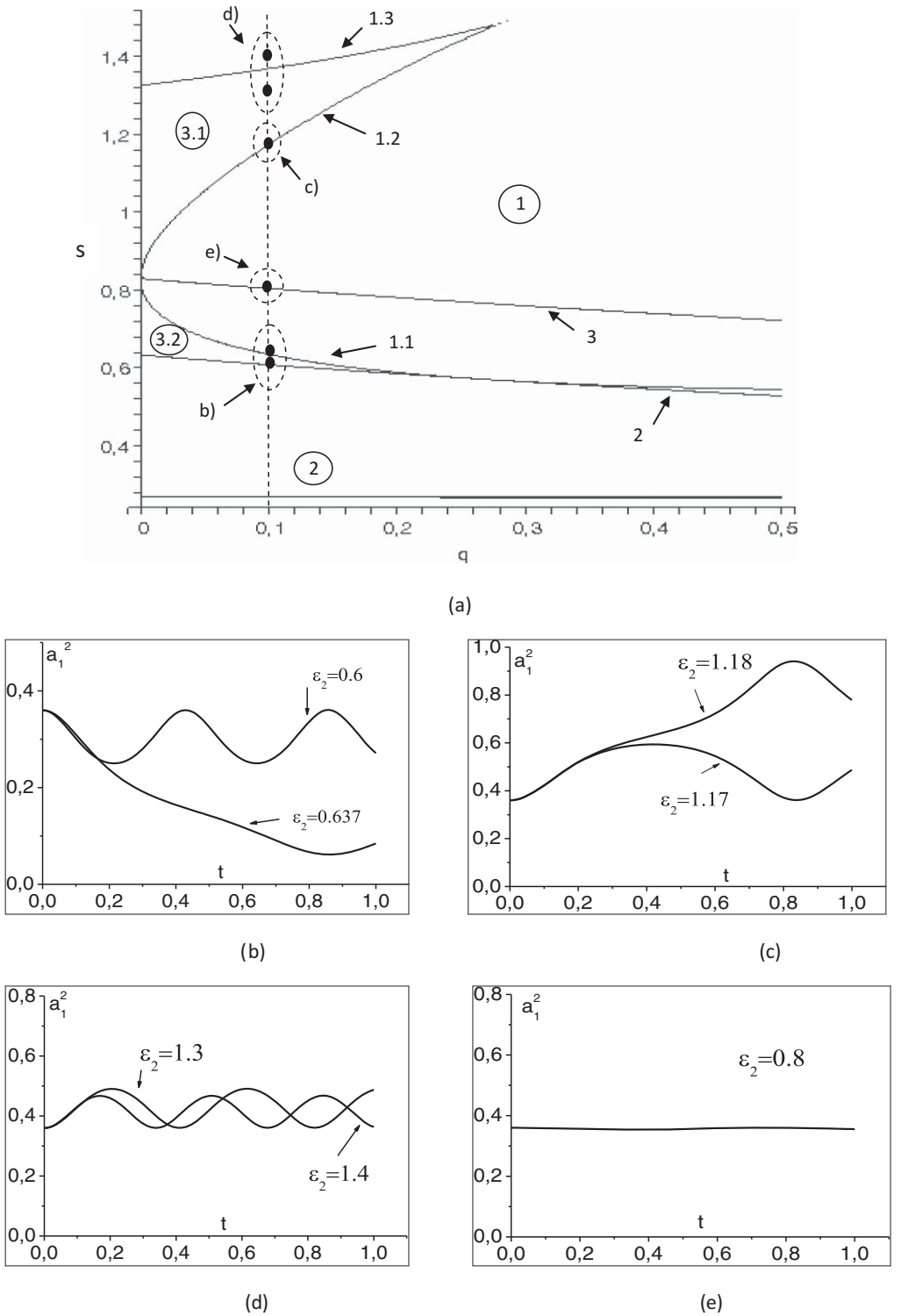

Fig. 5 Configuration of the regions (a) and evolution in time of the intensity of the fundamental wave for the parameters values in the vicinity of boundaries: (b) 1.1, (c) 1.2, (d) 1.3, and (e) curve 3 for $a_{10} = 0.6$, $a_{20} = 0.8$, and $\varphi_0 = 0$, $\alpha = 0.05$, $\gamma = 0.005$, $\varepsilon_1 = 1$ and values of ε_2 shown in the figures. Corresponding values of s and q are shown by dots and dashed circles in (a).

impossible. In this case, the intensity $P_1(t)$ of the fundamental wave oscillates according to the following rule [Fig. 4(a)]:

$$P_1(t) = \frac{(P_1)_1[(P_1)_2 - (P_1)_3] + (P_1)_2[(P_1)_1 - (P_1)_3] - h(P_1)_3[(P_1)_1 - (P_1)_2]}{[(P_1)_2 - (P_1)_3] + [(P_1)_1 - (P_1)_3] - h[(P_1)_1 - (P_1)_2]},$$

$$h = \sin\left\{\pm\frac{\alpha\beta I_1|r_0|}{\varepsilon_2}\sqrt{[(P_1)_1 - (P_1)_3][(P_1)_2 - (P_1)_3]}t + t'\right\}, \quad \begin{cases} "+", & 0 \le \varphi_0 < \pi \\ "-", & \pi \le \varphi_0 < 2\pi \end{cases},$$

$$t' = \arcsin\frac{[(P_1)_1 - (P_1)_0][(P_1)_3 - (P_1)_2] + [(P_1)_1 - (P_1)_3][(P_1)_0 - (P_1)_2]}{[(P_1)_1 - (P_1)_2][(P_1)_0 - (P_1)_3]}. \tag{25}$$

The half-period of the energy conversion is given by

$$\bar{t} = \frac{\varepsilon_2}{\alpha\beta I_1|r_0|}\frac{\pi}{\sqrt{[(P_1)_1 - (P_1)_3][(P_1)_2 - (P_1)_3]}}. \tag{26}$$

At the boundary between regions 2 and 3 (which is the part of curve 2), the two roots of the polynomial $f(x)$ is equal to zero and the choice of initial intensities of interacting waves corresponds to the following relation between the roots and $P_1(t)$: $(P_1)_4 = (P_1)_3 = 0 < (P_1)_2 \le P_1(t) \le (P_1)_1 < 1$. Then, the low-efficiency regime of SHG takes place with periodical dependence of $P_1(t)$ [Fig. 4(f)], which is determined by Eqs. (25) and (26) for $(P_1)_3 = 0$. Note that curve 2 is determined by

$$a_{20}\left[2qa_{10}^2\cos\varphi_0 + 2a_{10}^2a_{20}(2-s) + a_{10}^3(1-s^2)\right] = \frac{1-s^2}{s^2}\left(a_{10}^2 + a_{20}^2 s\right)^2.$$

To obtain this expression, we put $a_1 = 0$ in the expression for the modified invariant [Eq. (14)],

$$\tilde{\tilde{I}}_3 = a_2^4(1-s^2),$$

then express a_2^2 for $a_1 = 0$ from the first invariant [Eq. (11)]

$$a_2^2 = I_1/s$$

and take into account preservation of the first and the modified third invariants

$$\tilde{\tilde{I}}_3 = a_{20}\left[2qa_{10}^2\cos\varphi_0 + 2a_{10}^2a_{20}(2-s) + a_{20}^3(1-s^2)\right],$$

$$I_1 = a_{10}^2 + a_{20}^2 s.$$

If on the photonic crystal laser radiation falls only on the double frequency, then no energy conversion to the basic wave takes place for parameters from this part of curve 2 [line $P_1(t) = 0$ in Fig. 4(f)].

Essentially, region 2 includes curve 2, at which the 100% energy conversion of the fundamental wave is achieved (Figs. 2 and 3). For these parameters, one root of the polynomial is negative and two others are zero $(P_1)_4 < 0 = (P_1)_3 = (P_1)_2 < P_1(t) < (P_1)_1 < 1$. Hence, the intensity of the fundamental wave decreases from $(P_1)_0$ to 0 for $0 < \varphi_0 < \pi$ (Fig. 4(c)), while for $\pi < \varphi_0 < 2\pi$ it first grows up to $(P_1)_1$ and then decreases to 0. It changes in accordance with Eqs. (22) for $k = 2$ and $(P_1)_2 = 0$. A zero value of $P_1(t)$ is reached at the infinite moment of time with accordance to exponential law.

As mentioned above, curve 3 exists in the plane (q,s) for two values of the initial phase difference φ_0, which is equal to π and 0, and nonzero input intensity of the double-frequency wave. It is determined by

$$q\cos\varphi_0\left(a_{10}^2 + a_{20}^2 s\right) + 2a_{20}\left(a_{10}^2 + a_{20}^2 s\right)(2-s) - 3qsa_{20}^2\cos\varphi_0 + 2(s^2 - 4s + 1)a_{20}^3 = 0$$

$$\varphi_0 = 0,\ \pi$$

If φ_0 equals π, then part of curve 3 represents the boundary between subregions 3.1 and 3.2 of region 3 (Fig. 2). This is a result of the merging of boundary 1.1 with part of boundary 1.2 in the limit $\varphi_0 \to \pi$ (Figs. 2 and 3). In this case, because of choosing of a_{10}, the polynomial roots and intensity $P_1(t)$ are related as follows: $0 < (P_1)_4 < (P_1)_3 = P_1(t) = (P_1)_2 < (P_1)_1 < 1$ and the regime of unchanging initial intensities takes place. However, it is unstable in practice. That means that small perturbations of intensity lead to catastrophic changing of one. At the same time, the other part of curve 3, belonging to regions 3.2 and 2, corresponds to the stable regime of unchanging intensities. For its realization, it is necessary to choose the initial intensity of the fundamental wave in a special way. In this case, the polynomial roots and normalized intensity $P_1(t)$ are related as $0 < (P_1)_4 < (P_1)_3 < (P_1)_2 = P_1(t) = (P_1)_1 < 1$ in region 3.2, and $(P_1)_4 < (P_1)_3 < 0 < (P_1)_2 = P_1(t) = (P_1)_1 < 1$ in region 2. Note that in region 3.2, a high-efficiency regime of SHG can also take place. It occurs for certain initial intensities and corresponds to parameters q and s of boundary 1.3 between regions 1 and 3 [Fig. 4(e)]. Evolution of intensities is described by Eqs. (23) and (24).

For the zero value of the initial phase difference φ_0, curve 3 divides each of regions 1 and 2 into two parts. For parameters q, s, and a_{10} from curve 3 in region 1, there are two real roots of the polynomial $f(x)$, being equal each to other: $0 < (P_1)_2 = (P_1)_1 < 1$. The value of $P_1(t)$ is equal to them. In region 2. there are four real roots, but only two of them have physical meaning: $(P_1)_4 < (P_1)_3 < 0 < (P_1)_2 = (P_1)_1 < 1$. Similar to the previous case, due to the choice of a_{10} the normalized intensity of the basic wave is equal to the positive roots. In both cases, initial intensities of interacting waves stay constant and the stable regime of unchanging initial amplitudes takes place [Fig. 5(e)].

In the contrast to Ref. 29, the two line 4's, which are determined by conditions $s = 2 \pm \sqrt{3}$, exists in the plane (q,s). For the parameter values from these lines, the polynomial $f(x)$ has only three real roots: $(P_1)_1$, $(P_1)_2$, $(P_1)_3$. Two of them have physical meaning. For the initial intensity a_{10} corresponding to these situations, $P_1(t)$ belongs to the interval between the positive roots: $(P_1)_3 < 0 < (P_1)_2 \le P_1(t) \le (P_1)_1 < 1$. In this case, the evolution $P_1(t)$ oscillates [Fig. 4(a)] and is described by an elliptical sine,

$$P_1(t) = (P_1)_1 - h^2\left[(P_1)_1 - (P_1)_2\right],$$

$$h = sn\left[\frac{\beta\gamma\sqrt{I_1}}{\sqrt{\varepsilon_1\varepsilon_2}}\sqrt{(P_1)_1 - (P_1)_3}\,t - t'\middle| m\right],$$

$$t' = F(\theta_0|m)\begin{cases} 1, & 0 \le \varphi_0 < \pi \\ -1, & \pi \le \varphi_0 < 2\pi \end{cases},$$

$$\theta_0 = \arcsin\sqrt{\frac{(P_1)_1 - (P_1)_0}{(P_1)_1 - (P_1)_2}}, \quad m = \frac{(P_1)_1 - (P_1)_2}{\left[(P_1)_1 - (P_1)_3\right]},$$

with the half-period of oscillation as follows:

$$\bar{t} = \frac{\sqrt{\varepsilon_1\varepsilon_2}}{\beta\gamma\sqrt{I_1}}\frac{K(m)}{\sqrt{(P_1)_1 - (P_1)_3}}.$$

With parameters corresponding to the cuspidal point of the curve 1 (see Fig. 2), which is a common one of curves 1.1 and 1.3, for $\varphi_0 \neq \pi$, the coincidence of two positive roots of the polynomial takes place $0 < (P_1)_4 \le (P_1)_3 = (P_1)_2 = (P_1)_1 < 1$ and the evolution of $P_1(t)$, which varies between them, is given by

$$P_1(t) = \frac{h\,(P_1)_1 + (P_1)_4}{h+1},$$

$$h = \left\{\pm\frac{\alpha\beta I_1|r_0|}{2\varepsilon_2}[(P_1)_1 - (P_1)_4]t + t'\right\}^2,$$

$$\begin{cases} "-", & 0 \le \varphi_0 < \pi \\ "+", & \pi < \varphi_0 < 2\pi \end{cases}, \quad t' = \sqrt{\frac{(P_1)_0 - (P_1)_4}{(P_1)_1 - (P_1)_0}}.$$

For $\varphi_0 = \pi$, this point corresponds to the tangency one of curves 1 and 3 (the common point of curves 1 and 3). Then a regime of unchanging initial intensities takes place, which is unstable in practice.

For the parameters corresponding to the tangency point of curves 1 and 2 (the common point of curves 1.2, 1.4, and 2), the following relation of roots and intensity of the first wave $0 = (P_1)_4 = (P_1)_3 = (P_1)_2 \le P_1(t) \le (P_1)_1 < 1$ takes place and the energy conversion is described by

$$P_1(t) = (P_1)_1\frac{1}{h+1}, \quad h = \left[\pm\frac{\alpha\beta I_1|r_0|}{2\varepsilon_2}(P_1)_1\,t + t'\right]^2,$$

$$\begin{cases} "+", & 0 \le \varphi_0 < \pi \\ "-", & \pi \le \varphi_0 < 2\pi \end{cases}, \quad t' = \sqrt{\frac{(P_1)_1 - (P_1)_0}{(P_1)_0}}. \tag{27}$$

5 Results of Computer Simulation

In this section, we consider some examples of two-wave interactions with a layered structure to illustrate the validity of written solutions and to clarify the conditions of their application. For simplicity, we consider the evolution of SHG in the photonic crystal unbounded in the x coordinate. (This corresponds to situation when the length of crystal along the x coordinate is many times less than a diffraction length l_x of each subbeam in the domain of layer. This length is equal to $l_x = 2\pi\tilde{d}^2$, where $\tilde{d}$ is the smallest thickness of layers.) In this case, one can consider only 1-D photonic crystal. Hence, next we neglect a dependence of complex amplitudes on the x coordinate and do not take into account a propagation of laser pulses in the x direction. As a consequence of this, the initial distribution of complex amplitudes depends only on the z coordinate,

$$A_j(z, t=0) = A_{j0}A_0(z), \quad A_0(z) = e^{-(1/2)\{z-[L_z/1]/a\}^2},$$
$$j = 1, 2, \quad 0 \le z \le L_z, \tag{28}$$

with maximal amplitudes

$$A_{20} = 0.4, \quad A_{10} = \sqrt{1 - A_{20}^2}. \tag{29}$$

As follows from Eq. (28), the intensity of laser pulses is constant in time. Next, we discuss the evolution of intensity profiles in time and provide a comparison between the beam profiles calculated both from the analytical solution and computer simulation.

The first considered example corresponds to the case of equal layer lengths $d_1 = d_2 = 2$ with a large value of parameter $\Omega = 10^4$. This value corresponds to thickness of $d = 10^4\lambda_1$. Hence, for $\lambda_1 = 0.5\ \mu$m, $d_1 + d_2 = 2$ cm. Obviously, it is a very large structure for visible light. Nevertheless, for problems of frequency conversion of high-intensity pulses, this structure can be applied for the wide-aperture beam: the beam radius is ~0.5 m. For such a thickness of layers, the diffraction length is equal to 10^3 m. As one shows [Fig. 7(a)], the analytical solution is valid for $t \le 10$. This dimensionless value of time corresponds to 100 ps. Next, we will discuss, of course, the other ration d/λ. In all examples, the total number of layers is equal to 15.

Figures 6–10 show the evolution of the intensity profiles of fundamental and doubled-frequency waves, which were obtained due to computer simulation, for three sets of parameters. The first of them is characterized by proportional values of parameters for odd and even layers

$$\varepsilon_{11} = 1, \quad \varepsilon_{21} = 1.0395, \quad \alpha_1 = \gamma_1 = 10^{-4}, \text{ for odd layers},$$
$$\varepsilon_{12}=2, \quad \varepsilon_{22}=2\times1.0395, \quad \alpha_2=\gamma_2=2\times10^{-4}, \text{ for even layers}. \tag{30}$$

It should be stressed that the notations γ_1 and γ_2 refer to the layers and their values are the same for both equations. For the intensity at the axis of the beam, chosen parameters correspond to the point in curve 3 that corresponds to unchanging initial intensity (Fig. 2 for $\varphi_0 = \pi$), while the parameters for the other points of profile belong to region 2. Because of the negligible influence of diffraction on the time interval $0 \le t \le 1$, evolution of each point of the initial

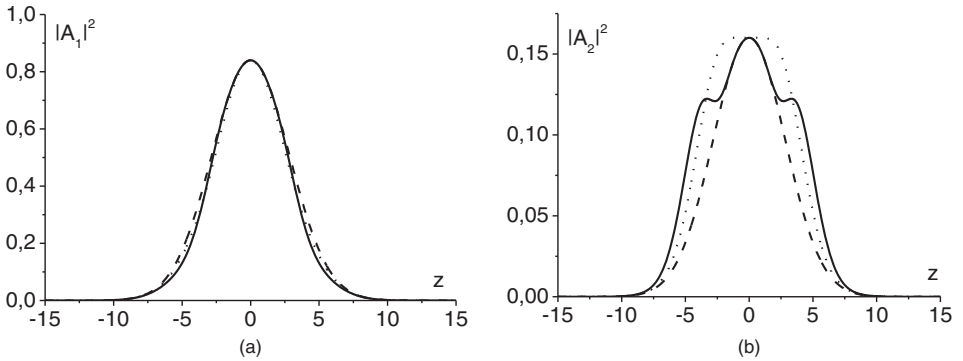

Fig. 6 Profiles of (a) intensity of the fundamental wave and (b) the wave with doubled frequency for $t = 0$ (dashed curves), 0.5 (dotted curves), 1 (solid curves). Parameters $\varepsilon_{11} = 1$, $\varepsilon_{21} = 1.0395$, $\alpha_1 = \gamma_1 = 10^{-4}$, $\varepsilon_{12} = 2$, $\varepsilon_{22} = 2 \times 1.0395$, $\alpha_2 = \gamma_2 = 2 \times 10^{-4}$, $A_{20} = 0.4$, $A_{10} = \sqrt{1 - A_{20}^2}$.

profiles is described by Eqs. (19)–(21). As a result, the intensity profiles of both waves approximately conserve their initial profiles [Figs. 6(a) and 6(b)]. Note that the same evolution is observed for $\Omega = 100$ (in this case, the thickness of layer is ~2 mm) and $\alpha_j = \gamma_j = 10^{-2}$ ($j = 1,2$), as well as for homogeneous media with parameters [Eq. (30)].

The second set the parameters of interacting waves

$$\varepsilon_{11} = \varepsilon_{12} = 1, \quad \varepsilon_{22} = 1.0395, \quad \varepsilon_{21} = 1.5,$$

$$\alpha_1 = \alpha_2 = \gamma_1 = \gamma_2 = 10^{-4}.$$

is also chosen in such a way that the intensity at the axis of the beam corresponds to the point in curve 3 (Fig. 2 for $\varphi_0 = \pi$). Other points of the beam belong to region 2. As a result, an intensity profile remains approximately constant in the even layers, including the intensity at the beam axis, while the interaction of beams in odd layers is characterized by significant energy conversion (Fig. 7). Hence, a different evolution of intensities for odd and even layers takes place and the intensity profiles reflect a crystal structure in a pronounced way (see profiles at $t = 2$ in Fig. 7).

For this set of parameters, we also made a comparison of the results of computer simulation to the analytical solutions for three values of parameter $\Omega = 10^4, 10^2, 10$, and three sets of quadratic and cubic nonlinearities: $\alpha_1 = \alpha_2 = \gamma_1 = \gamma_2 = 10^{-4}$ for $\Omega = 10^4$; $\alpha_1 = \alpha_2 = \gamma_1 = \gamma_2 = 10^{-2}$ for $\Omega = 10^2$; $\alpha_1 = \alpha_2 = \gamma_1 = \gamma_2 = 10$ for $\Omega = 10$ during the time interval that is equal to 10 dimensionless units. It should be stressed that the values $\Omega = 10^2$, 10 correspond to thickness

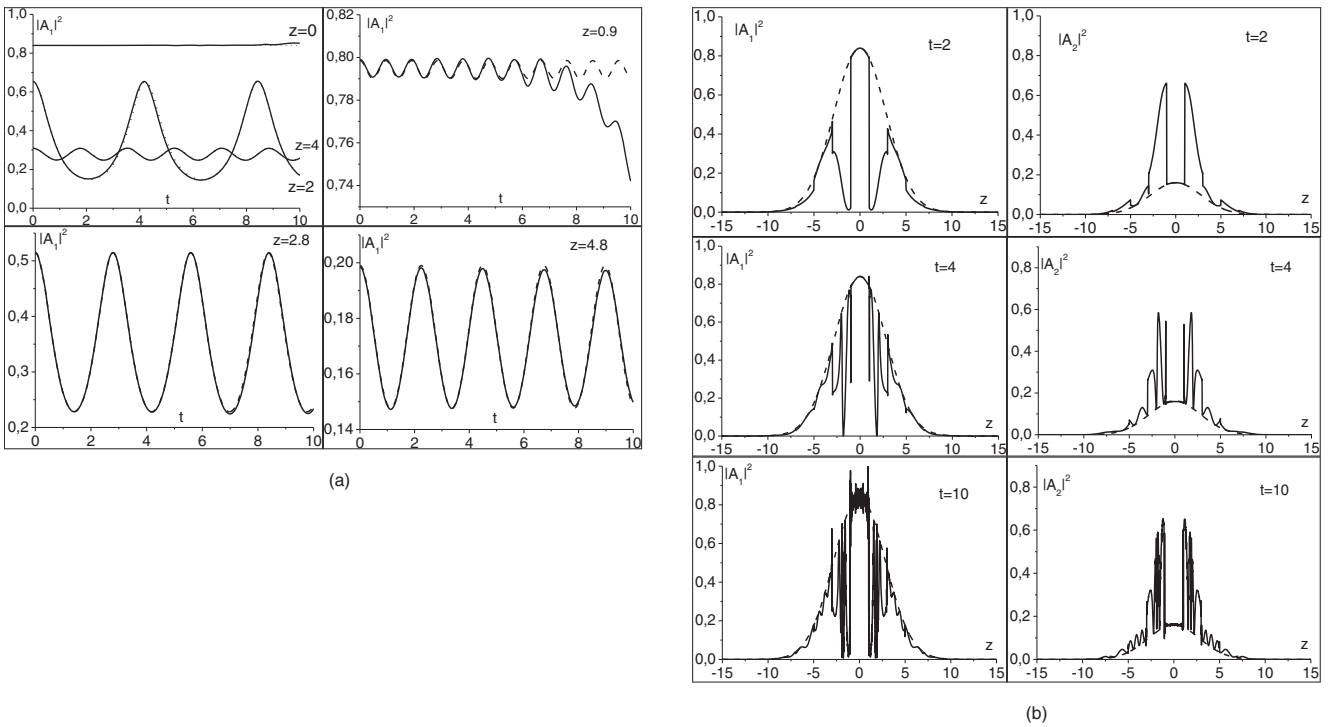

Fig. 7 Comparison of evolution of the intensity at the centers and near the edges of the layers for the fundamental wave: (a) computer simulation (solid curves) and theoretical results (dashed curves); (b) intensity profiles of the fundamental wave and of the doubled frequency wave at $t = 0$ (dashed curves) and at different times (solid lines). Parameters $\Omega = 10{,}000$, $\varepsilon_{11} = \varepsilon_{12} = 1$, $\varepsilon_{21} = 1.0395$, $\varepsilon_{21} = 1.5$, $\alpha_1 = \alpha_2 = \gamma_1 = \gamma_2 = 10^{-4}$ and $A_{20} = 0.4$, $A_{10} = \sqrt{1 - A_{20}^2}$.

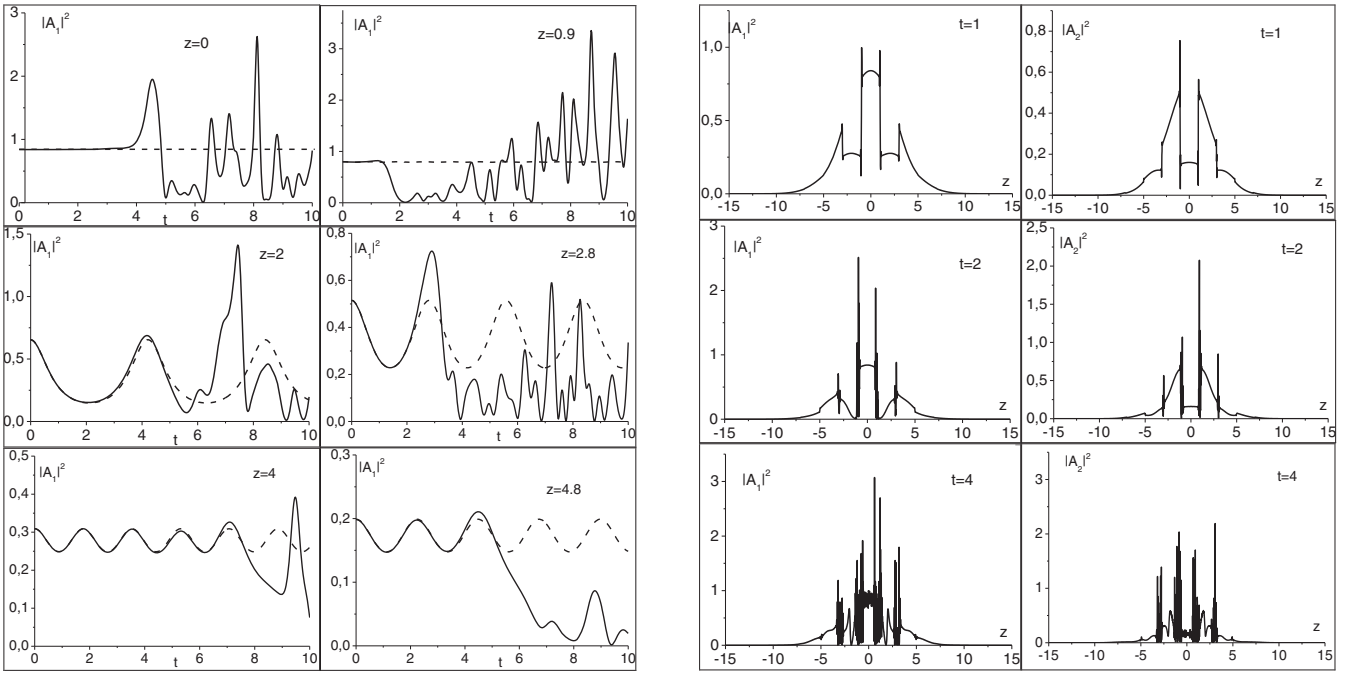

(a) (b)

Fig. 8 Comparison of evolution of the intensity at the centers and near the edges of the layers for the fundamental wave: (a) computer simulation (solid curves) and theoretical results (dashed curves); (b) intensity profiles of the fundamental wave and of the doubled frequency wave at different times. Parameters $\Omega = 100$, $\varepsilon_{11} = \varepsilon_{12} = 1$, $\varepsilon_{21} = 1.0395$, $\varepsilon_{21} = 1.5$, $\alpha_1 = \alpha_2 = \gamma_1 = \gamma_2 = 10^{-2}$ and $A_{20} = 0.4$, $A_{10} = \sqrt{1 - A_{20}^2}$.

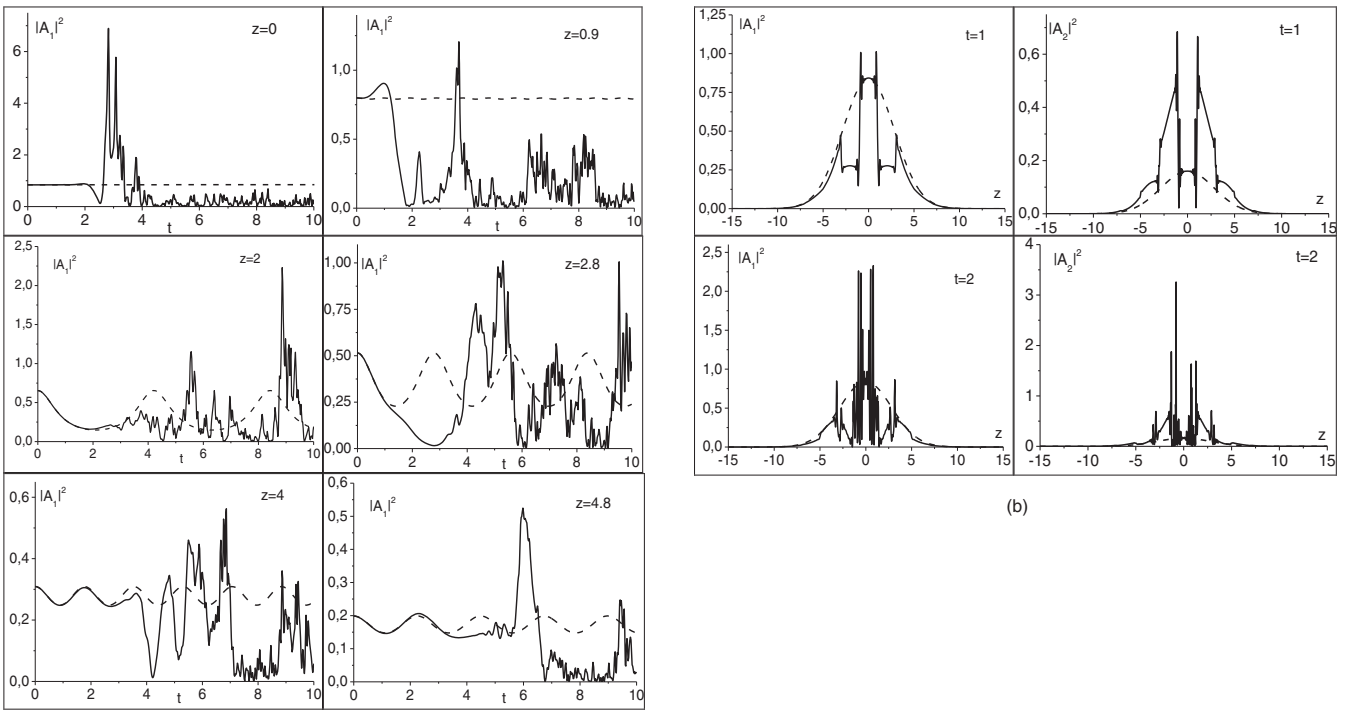

(a) (b)

Fig. 9 Comparison of evolution of the intensity at the centers and near the edges of the layers for the fundamental wave: (a) computer simulation (solid curves) and theoretical results (dashed curves); (b) intensity profiles of the fundamental wave and of the doubled frequency wave at $t = 0$ (dashed curves) and at different times (solid lines). Parameters $\Omega = 10$, $\varepsilon_{11} = \varepsilon_{12} = 1$, $\varepsilon_{21} = 1.0395$, $\varepsilon_{21} = 1.5$, $\alpha_1 = \alpha_2 = \gamma_1 = \gamma_2 = 10^{-1}$ and $A_{20} = 0.4$, $A_{10} = \sqrt{1 - A_{20}^2}$.

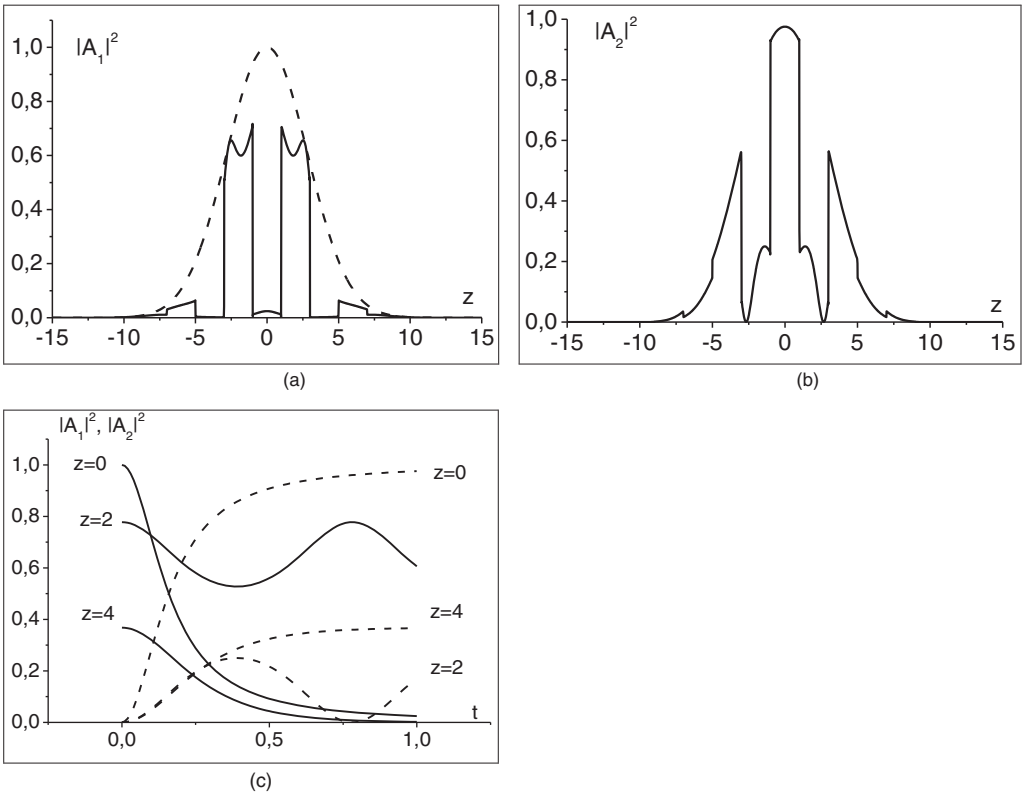

Fig. 10 Intensity profile of (a) the fundamental wave and (b) the doubled frequency wave for $t = 0$ (dashed curves), 0.5 (dotted curves), 1 (solid curves); (c) evolution of the intensity at the centers of the layers for the fundamental wave (solid curves) and for the SH waves (dashed curves). Parameters $\varepsilon_{11} = \varepsilon_{21} = \varepsilon_{12} = \varepsilon_{22} = 1$, $\alpha_1 = \alpha_2 = 2 \times 10^{-4}$, $\gamma_1 = 10^{-4}$, $\gamma_2 = 2 \times 10^{-4}$, $A_{20} = 0$, $A_{10} = 1$.

of layers 1 mm and 100 μm, correspondingly. On a time scale, these layer thicknesses correspond to 500 and 50 fs, correspondingly. Thus, the analytical solution can be valid at least for a layered structure with an approximate length of 5 cm, 5 mm, 500 μm for the three values of parameter Ω.

As is well seen from Figs. 7–9, the time interval for which analytical results coincide with the results of computer simulation depends on Ω and location of the point of intensity profile with respect to the layer's edge. Thus, for larger Ω the corresponding time interval is larger. It is also an increase for the points, corresponding to the center of the layer and for the points with coordinates far from the beam's center because of a decreasing intensity for these points. For example, a time interval of coincidence of the solutions is $\sim$10 dimensionless units for $\Omega = 10^4$; four units for $\Omega = 10^2$, and about two units for $\Omega = 10$ for the points at the axis beam ($z = 0$). Time intervals of the coincidence of analytical solution, with computer simulation results for the points in the center of the second ($z = 2$) and third layers ($z = 4$) are even greater. Thus, for $\Omega = 10^2$ and $z = 4$, the time interval is more than six dimensionless units; whereas for $\Omega = 10^2$ and $z = 4$, it is equal to three dimensionless units. At the edge of the central layer, which corresponds to the beam axis ($z = 0.9$), the time interval of validity of the analytical solution is about six units for $\Omega = 10^4$, about one unit for $\Omega = 10^2$, and $\sim$0.4 units for $\Omega = 10$. Corresponding values of the time interval during which the analytical solution is close to the computer simulation result for the edge of the second layer ($z = 2.8$) are 2 for $\Omega = 10^2$ and 1 for $\Omega = 10$. Whereas at the edge of the third layer ($z = 4.8$), they almost reach the values for the axis beam: four units for $\Omega = 10^2$ and about two units for $\Omega = 10$. Obviously, influence of diffraction of the beam, which is the most pronounced in the vicinity of the layers' edges, drastically disturbs the beam profile at $t = 10$ for $\Omega = 10^4$, $t = 4$ for $\Omega = 10^2$, and $t = 2$ for $\Omega = 10$.

Let us discuss in detail the influence of diffraction on the z coordinate on the beam profile evolution as a whole and intensity evolution for separate points on the z coordinate. As follows from Figs. 7–9 and the discussion above, small diffraction, which corresponds to $\Omega = 10^4$, allows neglecting the diffraction without considerable distortion of evolution of intensity profile during the considered time interval. Only areas where it becomes noticeable at the end of the time interval, are the edges of the central layer. The cause is a quite different evolution of intensities for the points from the odd and even layers, which follows from analytical consideration. Thus, the intensity profile remains approximately constant in the central layer, while oscillations of intensity with significant amplitudes takes place for the points corresponding to the boundaries with neighbor layers. As a result, the second-order derivatives on the z coordinate from amplitude distribution in the vicinity of the layers edges become so large that the corresponding terms in the equations should not be neglected, despite the small diffraction (determined by Ω).

It should be mentioned that the appearance of irregularity of the beam profile inside the layers arrises from dependence of the period of the intensity oscillation in time from the value of intensity at this point of the beam profile. The diffraction of the laser beam tends to suppress these

oscillations. As is well seen from Fig. 7, the diffraction of the beam tends to the redistribution of the light energy from the edges of the central layer to its center. This is also true for the points of the beam profile that are far from the central layer, including their edges because of relatively small intensities.

The time interval, for which the analytical solution is valid at computer simulation, decreases with growth of laser beam diffraction. It can be roughly estimated as two dimensionless units for $\Omega = 10^2$ and one dimensionless unit for $\Omega = 10$. Figures 8 and 9 show that the diffraction of the beam affects first at the edges of the central layers. As a result, the energy redistributes between the layer's edges and its center. Thus, the intensity evolution for separate points of the profile becomes far from a regular one. The same is valid for the layers close to the central one. Gradually, diffraction spreads its influence over other layers edges, causing the redistribution of energy and irregular behavior of evolution.

Figure 10 shows a comparison of computer simulation results to analytical solutions for the layers that are different in quadratic nonlinearity γ. For example, we suppose that the quadratic nonlinearities differed by a factor of 2 for the considered frequencies. The parameters for this case are

$$\varepsilon_{11} = \varepsilon_{21} = \varepsilon_{12} = \varepsilon_{22} = 1, \quad \alpha_1 = \alpha_2 = 2\times 10^{-4},$$
$$\gamma_1 = 10^{-4}, \quad \gamma_2 = 2\times 10^{-4}, \quad \Omega = 10^4.$$

At the initial moment of time, the SH wave is absent: $A_{10} = 1$, $A_{20} = 0$ and the parameters for all profile points lie in line 2 (Fig. 2). The point at the axis of the beam coincides with the common point of curves 1 and 2. For this point, as well as, for the other points belong to the central layer, the full energy conversion takes place [Eq. (27)] [Fig. 10(c), curves for $z = 0$]. For the points from the two layers, neighboring the central one, the parameters lie in the part of line 2, which is the boundary of regions 2 and 3. Thus, no full energy conversion takes place in these two layers [Fig. 10(c), curves for $z = 2$]. For the other layers, the full energy conversion is also realized [Fig. 10(c), curves for $z = 4$]. As a result, at $t = 1$, odd layers are characterized by the large intensity of the SH wave, while even layers are characterized by the large intensity of the fundamental wave [Figs. 10(a) and 10(b)].

6 Conclusion

We developed the theory of SHG in layered photonic crystal with combined nonlinearity in the framework of the plane-wave approximation. To obtain the solution, we use the invariants (conservation laws) of considered problem. The uniqueness and multiplicity of solutions of the problem are investigated. The evolution of solutions is attained in analytical formulas. Various modes of generation are obtained; among them one stresses the bistability mode, the mode of stabilization of initial amplitudes, and mode of full energy conversion. It is essential that without cubic susceptibility the appearance of a bistable regime of SHG is impossible.

We verified our analytical results on the base of the numerical simulation that was made for some examples. We demonstrated good agreement between analytical results and computer simulation results during the time interval, which depends on the parameters of the problem. We also provide estimations of sizes of photonic crystal and the time interval of the validity of the analytical solution.

Acknowledgments

This study was supported in part by the Russian Foundation for Basic Research (Project No. 09-02-00786-a).

References

1. J. Martorell and R. Corbalán, "Enhancement of second harmonic generation in a periodic structure with a defect," *Opt. Commun.* **108**(4–6), 319–323 (1993).
2. J. Martorell, "Parametric nonlinear interaction in centrosymmetric 3-dimensional photonic crystals,"*JOSA B* **19**, 2075–2082 (2002).
3. J. Trull, R. Vilaseca, J. Martorell, and R. Corbalán, "Second-harmonic generation in local modes of a truncated periodic structure," *Opt. Lett.* **20**(17), 1746–1748 (1995).
4. G. Bao and Z. Zhou, "Modeling of nonlinear optical second harmonic generation in periodic structures," in *Progress Analysis, Proc. of 3rd Int. ISAAC Congress*, pp. 1197–1106 (2001).
5. M. Okada, K. Takizawa, and S. Ieiri, "Second harmonic generation by periodic laminar structure of nonlinear optical crystal," *Opt. Commun.* **18**(3), 331–334 (1976).
6. M. Scalora, M. J. Bloemer, A. S. Manka, J. P. Dowling, C. M. Bowden, R. Viswanathan, and J. W. Haus, "Pulsed second harmonic generation in nonlinear, one-dimensional, periodic structures," *Phys. Rev. A* **56**, 3166–3175 (1997).
7. A. V. Balakin, V. A. Bushuev, N. I. Koroteev, B. I. Mantsyzov, I. A. Ozheredov, A. P. Shkurinov, D. Boucher, and P. Masselin, "Enhancement of second-harmonic generation with femtosecond laser pulses near the photonic band edge for different polarizations of incident light," *Opt. Lett.* **24**(12), 793–795 (1999).
8. M. A. Arbore, M. M. Fejer, M. E. Fermann, A. Hariharan, A. Galvanauskas, and D. Harter, "Frequency doubling of femtosecond erbium-fiber soliton lasers in periodically poled lithium niobate," *Opt. Lett.* **22**(1), 13–15 (1997).
9. M. Minamiguchi, M. Ashida, and T. Itoh, "Enhancement of quasi-phase-matched second harmonic generation with use of photonic band structure by optimizing densities of light mode," in *Nonlinear Optics: Materials, Fundamentals and Applications, Tech. Digest (CD)* Opt. Soc. of America, Paper No. WA4 (2004).
10. L.-X. Chen, D. Tang, W. Ding, and S. Liu, "High efficiency second harmonic generation in one-dimensional photonic crystal coupled cavity structures," *Opt. Eng.* **46**, 064602 (2007).
11. H. Tian, J. Tian, and Y. Ji, "Bright and dark solitons in quadratic nonlinear periodic structures and application to an all-optical logic gate," *J. Phys. B* **40**(7), 1391–1402 (2007).
12. R. G. Zaporozhchenko, "Compression and quasi-soliton propagation of femtosecond pulses in the regime of second harmonic generation in photonic crystals," *Opt. Spectrosc.* **99**(4), 522–526 (2005).
13. Y. Dumeige, F. Raineri, A. Levenson, and X. Letartre, "Second-harmonic generation in one-dimensional photonic edge waveguides," *Phys. Rev. E* **68**, 066617 (2003).
14. A. D'Orazio, D. de Ceglia, M. de Sario, F. Prudenzano, M. J. Bloemer, and M. Scalora, "Analysis of second harmonic generation in photonic-crystal-assisted waveguides," *J. Appl. Phys.* **100**(4), 043110 (2006).
15. W. Nakagawa, R.-Ch. Tyan, and Y. Fainman, "Analysis of enhanced second-harmonic generation in periodic nanostructures using modified rigorous coupled-wave analysis in the undepleted-pump approximation," *J. Opt. Soc. Am. A* **19**(9), 1919–1928 (2002).
16. D. Dumay, S. M. Saltiel, D. N. Neshev, W. Z. Krolikowski, and Yu. S. Kivshar, "Pulse measurements by randomly quasi phase matched second harmonic generation in the regime of total internal reflection," *J. Phys. B* **42**, 175403 (2009).
17. K. Rustagi, S. Mehendale, and S. Meenakshi, "Optical frequency conversion in quasi-phase-matched stacks of nonlinear crystals," *IEEE J. Quant. Elect.* **18**(6), 1029–1041 (1982).
18. S. M. Saltiel, W. Z. Krolikowski, D. N. Neshev, and Y. S. Kivshar, "Generation of Bessel beams by parametric frequency doubling in annular nonlinear periodic structures," *Opt. Express* **15**(7), 4132–4138 (2007).
19. N. Voloch, T. Ellenbogen, and A. Arie, "Radially symmetric nonlinear photonic crystals," *J. Opt. Soc. Am. B* **26**(1), 42–49 (2009).
20. S. M. Saltiel, D. N. Neshev, R. Fischer, W. Krolikowski1, A. Arie, and Y. S. Kivshar, "Generation of the secondharmonic conical waves via nonlinear Bragg diffraction," *Phys. Rev. Lett.* **100**, 103902 (2008).
21. K. Gallo and G. Assanto, "Spatial solitons in $\chi^{(2)}$ planar photonic crystals," *Opt. Lett.* **32**, 3149–3151 (2007).
22. K. Gallo, C. Codemard, C. B. Gawith, J. Nilsson, P. G. R. Smith, N. G. R. Broderick, and D. J. Richardson, "Guided-wave second-harmonic generation in a $LiNbO_3$ nonlinear photonic crystal," *Opt. Lett.* **31**, 1232–1234 (2006).
23. M. I. Molina and Yu. S. Kivshar, "Two-color surface solitons in two-dimensional quadratic photonic lattices," *JOSA B* **26**(8), 1545–1548 (2009).
24. S.-I. Inoue and Y. Aoyagi, "Ultraviolet second-harmonic generation and sum-frequency mixing in two-dimensional nonlinear optical polymer photonic crystals," *Jpn. J. Appl. Phys.* **45**, 6103–6107 (2006).

25. D. Antonucci, D. de Ceglia, A. D'Orazio, M. De Sario, V. Marrocco, V. Petruzzelli, and F. Prudenzano, "Enhancement of the SHG efficiency in a doubly resonant 2D-photonic crystal microcavity,"*Opt. Quant. Electron.* **39**(4-6), 353–360 (2007).
26. R. Fischer, D. N. S. M. Saltiel, A. A. Sukhorukov, W. Z. Krolikowski, A. Arie, and Y. S. Kivshar, "Pulse monitoring based on transverse SHG in periodic and disordered media," *Proc. SPIE* **6801**, 680110 (2008).
27. V. A. Trofimov, "Invariants of femtosecond pulse propagation in photonic crystals," *Comput. Math. Math. Phys.* **41**(9), 1358–1362 (2001).
28. T. M. Lysak and V. A. Trofimov, "Bistability and uniqueness of solutions in the problem of second harmonic generation of femtosecond pulses," *Comput. Math. Math. Phys.* **41**(8), 1214–1226 (2001).
29. T. M. Lysak and V. A. Trofimov, "Second harmonic generation by femtosecond pulses under the condition of nonzero amplitude of the double-frequency wave," *Opt. Spectrosc.* **93**(5), 797–809 (2002).
30. T. Ditmire, A. M. Rubenchik, D. Eimerl, and M. D. Perry, "Effects of cubic nonlinearity on frequency doubling of highpower laser pulses," *J. Opt. Soc. Am. B* **13**, 649–655 (1996).
31. S. Ashihara, J. Nishina, T. Shimura, and K. Kuroda, "Soliton compression of femtosecond pulses in quadratic media," J. Opt. Soc. Am. *B* **19**(10), 2505–2510 (2002).
32. V. M. Gordienko, S. S. Grechin, A. A. Ivanov, A. A. Podshivalov, and E. V. Rakov, "*Efficient parametric oscillation in the 8–10-μm range upon pumping by a femtosecond Cr:forsterite laser*," *Quantum Electron.* **36**(2), 114–116 (2006).
33. V. A. Trofimov and V. V. Trofimov, "High effective SHG of femtosecond pulse with ring profile of beam in bulk medium with cubic nonlinear response," *Proc. SPIE* **6610**, P6610R (2007).
34. Q. Wu and X.-C. Zhang, "Free-space electro-optic sampling of terahertz beam," *Appl. Phys. Lett.* **67**, 3523–3525 (1995).
35. X.-C. Zhang, "Three-dimensional terahertz wave imaging," *Phil. Trans. R. Soc. Lond. A* **362**, 283–299 (2004).
36. N. A. Vinokurov, B. A. Knyazev, G. N. Kulipanov, A. N. Matveenko, V. M. Popik, V. S. Cherkassky, and M. A. Shcheglov, "Visualization of radiation from a high-power terahertz free electron laser with a thermosensitive interferometer," *Tech. Phys.* **52**(7), 911–919 (2007).
37. N. Bloembergen, *Nonlinear Optics. A Lecture Note*, Harvard University, W. A. Benjamin, Inc., New York (1965).

Vyacheslav A. Trofimov graduated with honors from Lomonosov Moscow State University (Physical Department) in 1980 and where he obtained his PhD in laser physics in 1983 and, subsequently, his degree of Doctor of Science in 1995. He earned the title of senior researcher (computational mathematics) in 1990, professor (computational mathematics) in 1999, and honored professor in 2010 from Moscow State University. He subsequently worked as younger scientific researcher, scientific researcher, senior scientific researcher, leading scientific researcher, and the head of laboratory at the Laboratory of Mathematical Modeling in Physics, Faculty of Computational Mathematics & Cybernetics, Lomonosov Moscow State University. Since 1999, he is also a professor of the chair of Computational Methods Faculty of Computational Mathematics & Cybernetics Lomonosov Moscow State University. From 1998 to 2000, he was associated professor (part time) and from 2000 to 2002 as professor (part time) of the Chair of Chemistry Physics of the Department of Molecule and Biology Physics at Moscow Physics and Techniques Institute (State University). Since 1999, he was also professor (part time) of the Chair of Computational Mathematics in Moscow State University of Railways Communications (MIIT). His main field research experience includes laser physics, computer simulation, mathematical modeling, finite-difference scheme, programming, including multiprocessor computers. His current research interests include interaction of laser light with semiconductor, photonic crystal; propagation of terawatt laser pulse of femtosecond duration; frequency conversion of femtosecond pulse in medium with quadratic and cubic nonlinear response; optical bistability and 3-D optical memory; optical solitons; invariants and conservative finite-difference schemes for nonlinear Schrodinger equations, nonlinear and linear Maxwell's equations; terahertz spectroscopy and methods for getting instantaneous spectral response; electromagnetic properties of material with insertion of magnetic nanoparticles; computer simulation of growing of nitride-carbonate nanofilms; and application of THz radiation for the detection and identification problems. He has received the Lenin Komsomol Prize (physics), USSR, in 1987, Soros Professor award (ISSE Program) in 2000 to 2001, and State Scientific Grant, Russia, from 2000 to 2003. He was an invited speaker at 25 conferences and published over 385 papers (excluding abstracts of conferences reports and preprints). Total number of his publications is 600, communications to scientific meetings (in Russia and abroad), about 145. He has supervised 13 PhD candidates in the sciences (physics and mathematics).

Tatiana M. Lysak graduated with honors from Lomonosov Moscow State University (Physical Department) in 1985 and obtained her PhD in calculus mathematics from the same university in 1990. She subsequently worked as younger scientific researcher, scientific researcher, and senior scientific researcher (present time) in the Laboratory of Mathematical Modeling in Physics, Faculty of Computational Mathematics and Cybernetics of Lomonosov Moscow State University. Her research interests include interaction of laser light with semiconductor, photonic crystal, frequency conversion of femtosecond pulse in medium with quadratic and cubic nonlinear response, optical bistability, and optical solitons.

Biography and photograph of the other author not available.